Pseudo-irreversible butyrylcholinesterase inhibitors: structure–activity relationships, and kinetic, computational, and crystallographic study of the *N*-dialkyl *O*-arylcarbamate warhead

Anže Meden[a], Damijan Knez[a], Xavier Brazzolotto[b], Fabrice Modeste[c], Andrej Perdih[a,d], Anja Pišlar[e], Maša Zorman[a], Maja Zorović[f], Milica Denic[b], Stane Pajk[a], Marko Živin[f], Florian Nachon[b], Stanislav Gobec*[a]

[a]*University of Ljubljana, Faculty of Pharmacy, Department of Pharmaceutical Chemistry. Aškerčeva 7, SI-1000 Ljubljana, Slovenia.*
e-mail: stanislav.gobec@ffa.uni-lj.si

[b]*Institut de Recherche Biomédicale des Armées, Département de Toxicologie et Risques Chimiques, Unité Neurotoxiques. 91223 Brétigny sur Orge, France.*

[c]*Institut de Recherche Biomédicale des Armées, Département des Plateformes et Recherches Technologiques, Unité Développements Analytiques et Bioanalyse. 91223 Brétigny sur Orge, France.*

[d]*National Institute of Chemistry, Hajdrihova ulica 19, SI-1000 Ljubljana, Slovenia*

[e]*University of Ljubljana, Faculty of Pharmacy, Department of Pharmaceutical Biology. Aškerčeva 7, SI-1000 Ljubljana, Slovenia.*

[f]*Faculty of Medicine, Institute of Pathological Physiology, University of Ljubljana, SI-1000 Ljubljana, Slovenia*

Abstract

Alongside reversible butyrylcholinesterase inhibitors, a plethora of covalent butyrylcholinesterase inhibitors have been reported in the literature, typically pseudo-irreversible carbamates. For these latter, however, most cases lack full confirmation of their covalent mode of action. Additionally, the available reports regarding the structure–activity relationships of the *O*-arylcarbamate warhead are incomplete. Therefore, a follow-up on a series of pseudo-irreversible covalent carbamate human butyrylcholinesterase inhibitors and the structure–activity relationships of the *N*-dialkyl *O*-arylcarbamate warhead are presented in this study. The covalent mechanism of binding was tested by IC_{50} time-dependency profiles, and sequentially and increasingly confirmed by kinetic analysis, whole protein LC-MS, and crystallographic analysis. Computational studies provided valuable insights into steric constraints and identified problematic, bulky carbamate warheads that cannot reach and carbamoylate the catalytic Ser198. Quantum mechanical calculations provided further evidence that steric effects appear to be a key factor in determining the covalent binding behaviour of these carbamate cholinesterase inhibitors and their duration of action. Additionally, the introduction of a clickable terminal alkyne moiety into one of the carbamate *N*-substituents and *in situ* derivatisation with azide-containing fluorophore enabled fluorescent labelling of plasma human butyrylcholinesterase. This proof-of-concept study highlights the potential of this novel approach and for these compounds to be further developed as clickable molecular probes for investigating tissue localisation and activity of cholinesterases.

Introduction

In addition to the well-known acetylcholinesterase (AChE), another enzyme can terminate cholinergic transmission in the human body: human butyrylcholinesterase (hBChE).[1] Due to its lower substrate specificity, hBChE can hydrolyse a number of different esters – e.g., hunger-hormone ghrelin, cocaine and heroin, among others, although its precise physiological role still remains a mystery. Over the last three decades, BChE has emerged as an interesting and well-explored target in the medicinal chemistry community, especially in the fields of neurodegenerative diseases (predominantly Alzheimer's disease), bioscavanging organophosphorous nerve agents, inactivation of cocaine, heroin overdose prevention, and ghrelin-mediated effects on body weight.[1–9] The BChE active site can be separated into several defined regions: the catalytic triad (Ser198, His438, Glu325); the oxyanion hole (Gly116, Gly117, Ala199); the choline-binding pocket (Trp82); and the acyl-binding pocket (Trp231, Leu286, Val288, Phe329). Near the entrance to the active site gorge there is the putative peripheral site, made of residues Asp70 and Tyr332.[1,2]

Leaving a superabundance of classic reversible BChE inhibitors (BChEIs) aside, different cholinesterase inhibitor (ChEI) classes that feature carbamate moieties have been reported in the literature – e.g., *Scheme 1:* derivatives of physostigmine (**1a**,), isosorbide, tetrahydroquinazoline (**1b**, **1d**), phenothiazine, xanthone, chalcone, coumarin, resveratrol, *N*-substituted piperidine and piperazine, indole (**1c**), and others; these were well-covered in a recent review that highlighted their potential multifunctionality.[10] Furthermore, the first ChEI discovered was indeed the plant alkaloid physostigmine **1a**, where its covalent pseudo-irreversible mechanism of action through a carbamate warhead was only later realised.[11]
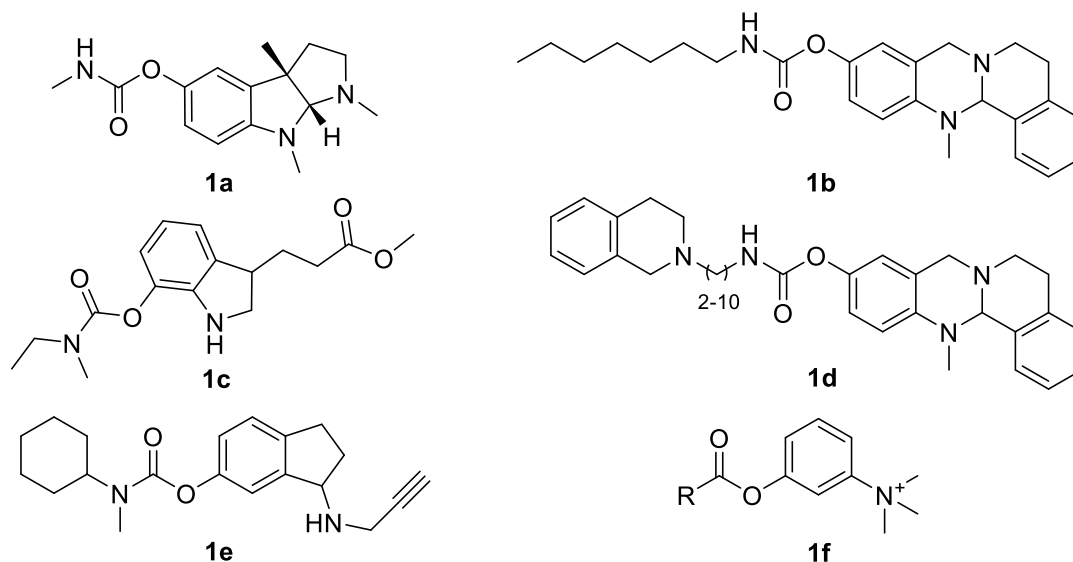
Scheme 1: Representative carbamate cholinesterase inhibitors from the literature.

The introduction of a carbamate warhead (most often the ethylmethyl carbamate of rivastigmine[12] as in **1c** or phenyl carbamate) on a variety of scaffolds easily produces BChEIs. However, a word of caution: especially in the field of cholinesterases, the literature is filled with examples of "IC$_{50}$-value-only" ChEIs that lack full and correct confirmation of their covalent modes of action. Taking advantage of the BChE broad substrate recognition and promiscuous binding due to the large, hydrophobic active site, such compounds can easily bind

reversibly with micromolar affinities. An example from our research group[13] nicely shows that the presence of the carbamate moiety in a BChE-active compound does not simply guarantee a covalent mechanism of action. As with all of the other covalent inhibitors, the carbamate inhibitors must also be carefully optimised, in terms of both electrophilicity and reactivity of the warhead itself, and with regards to the correct orientation and steric requirements that allow for the covalent modification to proceed.[14–19]

Although IC_{50} values do not allow for a full characterisation of covalent inhibitors, within a series of compounds. a comparison of the ligand IC_{50} values at a fixed timepoint can be both valid and rapid in a fast-moving drug discovery programme compared to the determination of the exact k_{inact}/K_I values.[20] In our hands, the following "triage" of testing potential covalent inhibitors is used: the IC_{50} values are determined at different timepoints to ascertain the time-dependency profile (decreasing IC_{50} values with longer preincubation times are indicative of a special mechanism of binding[21]), the hits with pronounced or inconclusive time-dependent profiles are then confirmed by kinetic analysis (*via* k_{obs} from initial velocity measurements[22–24] or full progress curve analysis[25]), with the final unequivocal proof provided by crystallisation or LC-MS, or both.

To date, only a handful of studies have investigated the structure-activity relationships (SARs) and kinetic characterisation of pseudo-irreversible carbamate ChEIs, with earlier efforts focused on the isocyanate-derived <u>monosubstituted</u> aryl carbamates, such as physostigmine (**1a**) derivatives.[26,27] The Decker group has repeatedly reported on a series of evodiamine-derived BChEIs that among other interesting properties also feature a <u>monosubstituted</u> carbamate warhead. Following up on the representative *n*-heptyl carbamate **1b**[28,29], *N*-monosubstituted carbamates with a terminal basic heterocyclic or tertiary amine (e.g., **1d**, *Scheme 1*) on a 2–10 carbon atom spacer had an extended duration of action (1–28 h), which was attributed to the interaction of the ω-moiety with the peripheral site.[22] Groner et al. used two series of <u>disubstituted</u> *N*-alkyl-*N*-methyl carbamates with two different leaving group scaffolds to show that carbamoylation rates of hAChEs are mainly influenced by the size and number of degrees of freedom of the *N*-alkyl (R) substituent, while for hBChE, the rates were more dependent on the structure of the leaving group. Decarbamoylation rates were greater for hBChE than for hAChE, and also less dependent on the size of R. For hBChE, the dimethylcarbamoylated enzyme recovered the fastest. Interestingly, the bulkier *N*-cyclohexyl-*N*-methyl carbamate **1e** was inactive.[23] Temperature also had a substantial impact on the decarbamoylation rate.[12] For AChE, Venkatasubban and co-workers reported on a series of monomethyl, dimethyl, ethyl methyl and diethyl carbamates with different leaving groups (phenols, fluoride). Due to long recovery times (up to several weeks), radiolabelling the hAChE and calculation of the final substrate turnover rate was necessary to accurately determine the decarbamoylation constants within a reasonable timeframe (up to 24 h). The increase in carbamate size by adding further *N*-methyl or *N*-ethyl groups had a significant impact on the decarbamoylation rates of **1f**, with the approximate ratios $H_2N : MeNH : Me_2N : EtMeN : Et_2N = 8000 : 800 : 200 : 10 : 1$.[30]

Moreover, AChE and BChE can be used as biomarkers for detection of Alzheimer's disease[1,31,32], Hirschsprung's disease[33,34] and multiple sclerosis.[35,36] To date, only a few AChE[37–42] and BChE[43–45,45–47] fluorescent probes and histochemical methods[48] have enabled tissue ChE location and activity determination. Accordingly, the development of new chemical probes for investigating the roles of ChEs in physiological and pathophysiological processes *in vitro* and *ex vivo* is required by biologists and neurobiologists.[49–51]

In a previous publication[52] we reported successful conversion of tryptophan-derived sp^3-rich selective hBChE inhibitors into pseudo-irreversible inhibitors through the introduction of a

carbamate moiety that enabled covalent binding to the target and prolonged the inhibition (*Scheme 2*). In the present study, we follow up on this series of pseudo-irreversible covalent carbamate hBChE inhibitors and report on their SARs, selectivities, and potential to be used as clickable molecular probes for fluorescent labelling of ChEs.
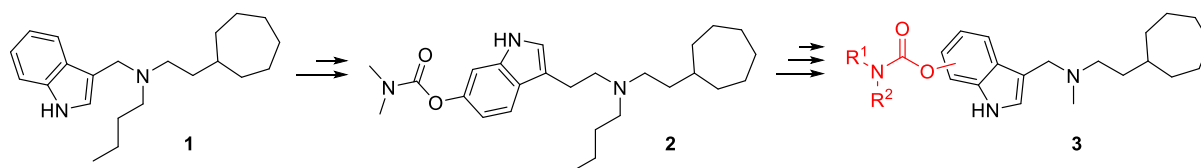

Scheme 2: Conversion of reversible selective hBChE inhibitor **1** scaffold[52] to a pseudo-irreversible covalent carbamate inhibitor **2**[52] and the structure–activity relationship of the carbamate warhead (general structure **3**).

Design and Chemistry

Non-covalent fluorophore-labelled ChEIs have significantly lower affinities and specificities towards ChEs because the fluorophore usually does not contribute significant new interactions within the active site. A substantial portion of the fluorophore is free and in equilibrium with the bound inhibitor in the active site. Additionally, it can bind to tissue samples in a non-specific manner. The former is responsible for high background fluorescence and the latter for artefacts in the microscopy imaging.

To improve the selectivity of probes, the following approach can be used that has not yet been reported in the literature: a "clickable" moiety (i.e., alkyne) at the carbamate warhead is transferred and pseudo-irreversibly bound in the ChE active site, while the unbound inhibitor and the leaving group can be effectively removed by washing, leaving only the "clickable" alkyne[53,54] on the protein of interest to be labelled in the next step *via* the copper(I)-catalysed click reaction (i.e., copper-catalysed azide-alkyne cycloaddition) with an azide-functionalised fluorophore (*Scheme 3*). *In situ* click chemistry has already been shown to be a valuable tool in the discovery of potent AChE inhibitors.[55–57]
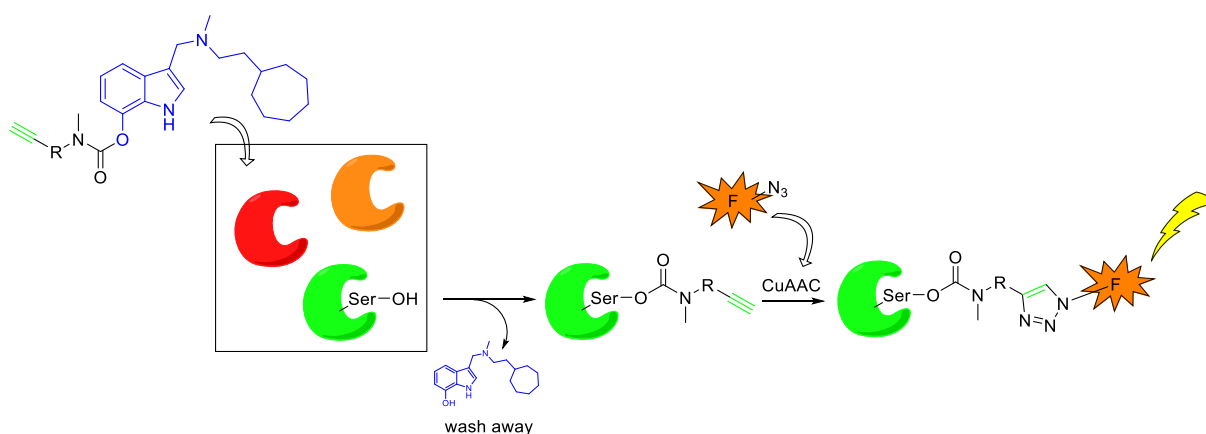
Scheme 3: The proposed labelling of ChEs with a carbamate warhead and subsequent copper-catalysed azide-alkyne cycloaddition click derivatisation with a fluorophore.
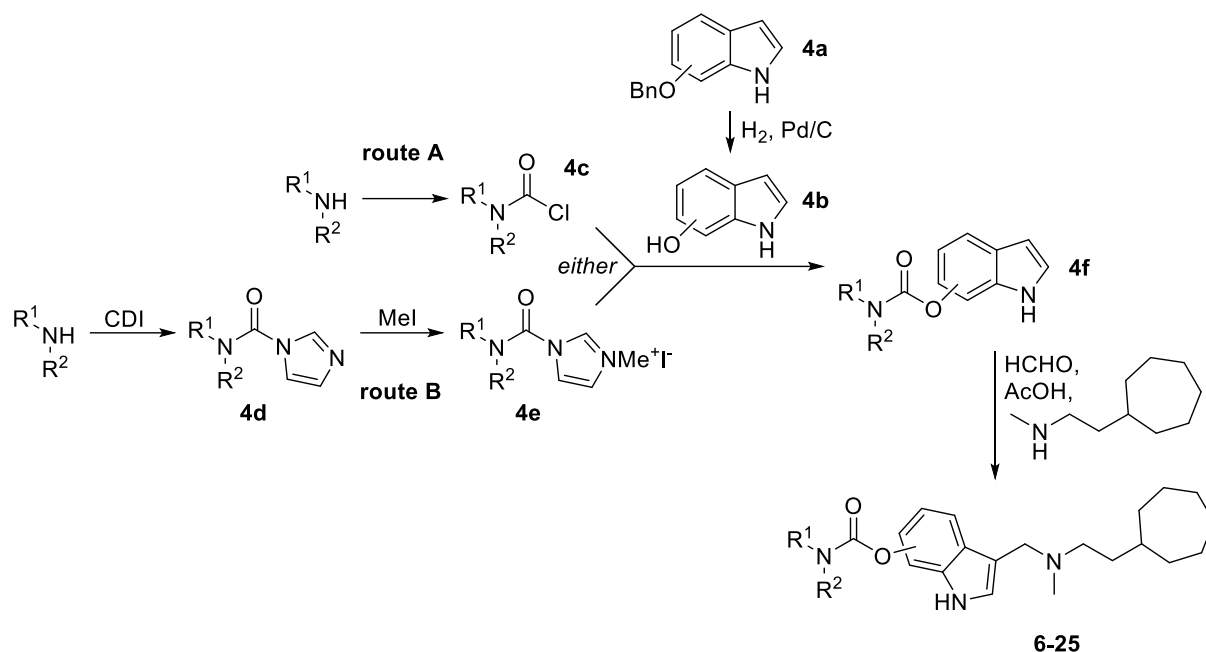
Scheme 4: General synthetic route from disubstituted amines to carbamate end compounds.

The required, air-sensitive 6- or 7-indolols **4b** were prepared *ex tempore* from commercially available benzyloxyindoles **4a** though hydrogenolytic debenzylation. Apparently straightforward carbamoylation with carbamoyl chlorides **4c** (route A, *Scheme 4*) in the presence of different bases led to a mixture of products. Presumably *C*3-alkylation is facile, as well, due to the electron-rich character of these indolols. Therefore, a cleaner alternative was sought – route B *via N,N*-dialkylcarbamoylimidazolium[58] salts **4e** in the presence of *N,N*-diisopropylethylamine (DIPEA) provided only the desired *O*-carbamoylated product **4f**. This route offers additional advantages; for instance, the greater commercial availability of disubstituted amines *vs*. carbamoyl chlorides, it avoids the use of highly toxic (di-, tri-)phosgene, and is also exceptionally mild and therefore suitable for sensitive or polyfunctional amines (e.g., as in **21, 22**). The final compounds were then facilely prepared in one additional step – Mannich reaction of indole carbamates **4f** with formaldehyde and 2-cycloheptyl-*N*-methylethan-1-amine in acetic acid at room temperature. This last reaction step was carefully chosen to allow for gentle reaction and isolation conditions – namely, the absence of strong acids or bases, which could destroy labile electrophilic warheads.

Results and Discussion
Inhibition of Cholinesterases

The reversible inhibitor scaffold that was optimal in terms of potency and selectivity was retained from the previous series[52], with only the *n*-butyl substituent on the central amine replaced by a methyl group, to balance the lipophilicity (*Scheme 2*). We have already established that positions 6 and 7 on the indole ring are suitable for the introduction of the carbamate warhead, and therefore only 6- and 7-substituted indolyl carbamates were designed and compared (*Tables 1–3, Figures 1, S1–2*).
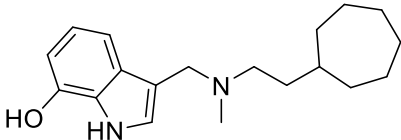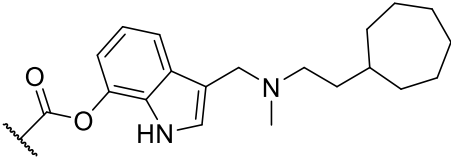
As expected, the leaving group for 7-substituted indolyl carbamates, **5**, had a decreased inhibitory potency compared to deshydroxy analogues[52], as the polar 7-hydroxy group occupies the highly lipophilic acyl-binding pocket (*Table 1*). The archetypal dimethyl carbamate **6** had single digit nanomolar affinity and a roughly 300-fold higher selectivity for hBChE over
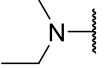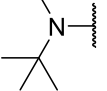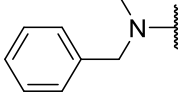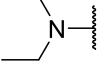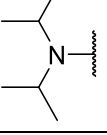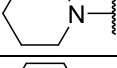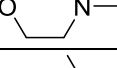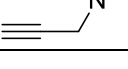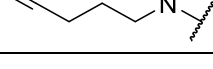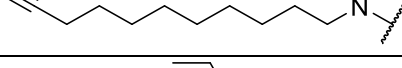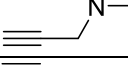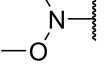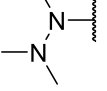
hAChE. Replacing one of the methyls with larger substituents – e.g., ethyl in **7**, isopropyl in **8**, *tert*-butyl in **9** and benzyl in **10**, led to decreased potency, except in the case of benzyl methyl carbamate **10**, where the benzyl group appeared to favourably interact with aromatic residues either in the acyl- or choline-binding pocket. The increased steric bulk of **9** *tert*-butyl precluded the carbamoylation of the catalytic Ser198. Increasing the steric repulsion further, the diethyl analogue **11** had an approximately 30-fold decreased affinity *vs.* parent compound **6**; however, it selectively carbamoylated only hBChE (*Figure 1*). The selectivity factor for hAChE was only 90, nevertheless the differential duration of action intertwined with PD-PK processes might be worth exploring further. The bulkiest diisopropyl carbamate **12** lost the ability to carbamoylate either of the ChEs. Locking the flexible diethyl substituent in a six membered ring (**13**, **14**) decreased the steric factors back to the level of ethyl methyl carbamate.

With a possibility of click derivatisation and fluorescent labelling of hBChE in mind, we also introduced a terminal alkyne into one of the carbamate substituents – e.g., replaced Me with propargyl in **15**, pent-4-yn-1-yl in **16** and undec-10-yn-1-yl in **17**. This led to clickable analogues with steric demands comparable to **7**, with **17** benefitting from additional van der Waals interactions. The increased steric bulk might have shifted the selectivity profile completely towards hBChE, as in **11**; therefore, compounds **18**, **19** and **20** with the ethyl, propargyl and isopropyl propargyl carbamate moiety were synthesised and tested. However, the selectivity factor did not exceed 350.

As both carbamoylation and decarbamoylation are dependent on both steric and electronic factors, two other interesting analogues were prepared: with methoxy (**21**) and dimethylamino (**22**) substituents on the carbamate nitrogen (*Table 1*). The electron-withdrawing character of these substituents should increase both de- and carbamoylation rates. Indeed, when we tried to ascertain the rate constants through k_{obs} measurements, fast reactivation precluded the separation of the carbamoylation and decarbamoylation phases. Therefore, these two compounds are better described as slow substrates.
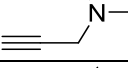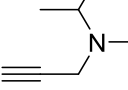
Table 1: *In vitro* ChE inhibitory potencies of 7-substituted indolyl carbamates (compounds **6**–**22**) and their leaving group (compound **5**).

Structure	Compound	hBChE	hAChE
		$IC_{50} \pm SEM$ [nM][a] 5-min preincubation	
		Time-dependency observed: yes/no	
	5	373.3 ± 53.1	11593 ± 2676
General structure:			
	6	1.76 ± 0.04	558.6 ± 98.7
		yes	yes

Structure	#		
	7	10.41 ± 2.99	6816 ± 1261
		yes	yes
	8	114.2 ± 15.3	2833 ± 346
		yes	yes
	9	147.0 ± 9.0	10042 ± 2183
		no	no
	10	11.59 ± 1.76	531.2 ± 16.9
		yes	yes
	11	60.95 ± 5.95	5590 ± 374
		yes	no
	12	230.1 ± 30.9	4629 ± 724
		no	no
	13	5.28 ± 0.55	529.1 ± 45.6
		ambiguous	yes
	14	11.42 ± 0.56	3584 ± 1182
		ambiguous	yes
	15	7.75 ± 1.45	340.3 ± 20.2
		ambiguous	yes
	16	12.29 ± 2.01	1081 ± 65
		yes	yes
	17	3.773 ± 0.804	123.2 ± 17.9
		yes	yes
	18	21.94 ± 3.49	7526 ± 1047
		yes	yes
	19	32.75 ± 3.18	464.1 ± 38.2
		ambiguous	yes
	20	80.49 ± 15.51	5354 ± 994
		no	no
	21	157.9 ± 16.05	1101 ± 130
		ambiguous	no
	22	13.15 ± 3.40	5560 ± 1029
		yes	yes

[a] SEM – standard error of the mean; data are means of two independent experiments, each performed in triplicate.
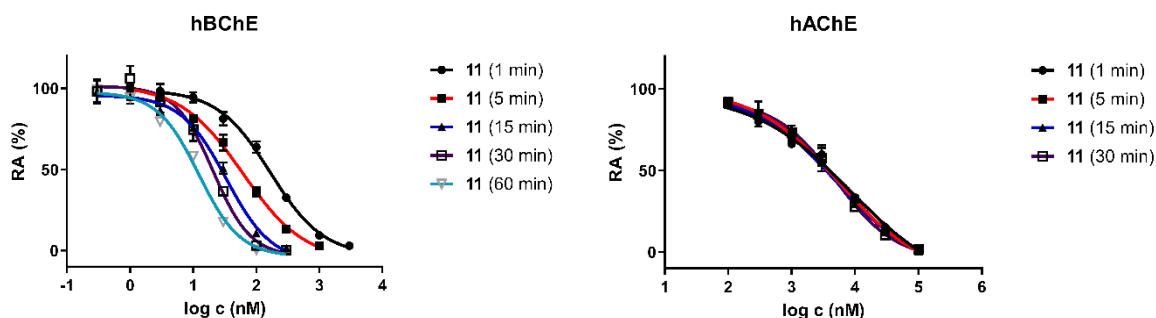
Figure 1: Time-dependency of hBChE (left) and hAChE (right) inhibition for diethyl carbamate inhibitor **11**. Residual activities (RAs) are plotted against log-concentrations. The leftward shift – the decreasing IC_{50} values with longer preincubation times – suggests the covalent mechanism of inhibition, as in the case of hBChE (left). Data from other time–dependency experiments can be found in Supporting Information.

To better understand the steric factors that affect the covalent mechanism of binding, we also tested the fragment-sized synthesis intermediates **6a**, **7a**, **12a** and **14a** (*Table 2, Figure S2*). The fragments displayed non-negligible reversible binding affinities, as seen in **12a** and **14a**. This latter is especially interesting as it lacks the pseudo-irreversible inhibition character of the full-sized inhibitor **14**, which shows that the rest of the molecule that directs the warhead into an appropriate position using reversible interactions can be an equally important factor that governs the activity of covalent inhibitors.[59]

Table 2: *In vitro* ChE inhibitory potencies of carbamate fragments.

Structure	Compound	hBChE $IC_{50} \pm SEM$ $[\mu M]^a$ 30-min preincubation	hAChE $RA[\%]^b$ at 100 µM after 30-min preincubation
		Time-dependency observed: yes/no	
	6a	1.66 ± 0.09	$2.4 \pm 0.6\%$
		yes	yes
	7a	1.39 ± 0.06	$56.2 \pm 5.4\%$ Not active
		yes	
	12a	12.78 ± 3.42	$66.5 \pm 5.6\%$ Not active
		no	
	14a	2.39 ± 0.91	$19.3 \pm 1.3\%$

		no	ambiguous
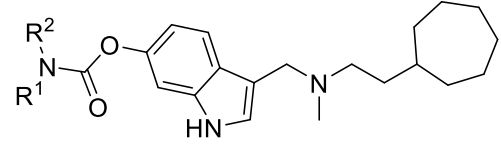
[a]SEM – standard error of the mean; data are means of two independent experiments, each performed in triplicate.
[b]RA – residual activity (mean ± standard deviation of one independent experiment performed in triplicate).
hAChE RA at 100 µM after 30 min preincubation

To design selective covalent carbamate hBChE inhibitors, we also prepared a series of 6-substituted indolyl carbamates, as this approach has been successful before.[52] The dimethyl carbamate **23** inhibited both ChEs and had decreased potency compared to the 7-substituted analogue **6**. Increasing the steric bulk led to compounds that lost the ability to covalently modify the enzyme (*Table 3*).

Table 3: *In vitro* ChE inhibitory potencies of 6-substituted indolyl carbamates (compounds **23**–**25**).

General structure		Compound	hBChE	hAChE
			$IC_{50} \pm SEM$ [nM][a] 5-min preincubation	
R^1=	R^2=		Time-dependency observed: yes/no	
Me	Me	**23**	45.62 ± 5.66	6719 ± 1377
			yes	yes
iPr	iPr	**24**	86.23 ± 18.04	336.5 ± 37.8
			no	no
propargyl	Me	**25**	10.15 ± 2.15	1456 ± 138
			no	no

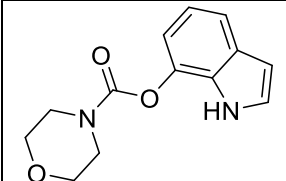[a]SEM – standard error of the mean; data are means of two independent experiments, each performed in triplicate.

To support the covalent mechanism of binding with kinetic evidence, the carbamoylation rate constant (k_{carb}) and inhibitory constant for the reversible binding K_i were determined for **6** from pseudo-first order inhibition rates (k_{obs}) (*Figure 2, Table 4*). The carbamate reversibly binds with low nanomolar affinity to the enzyme before the carbamoylation takes place.

Decarbamoylation rate constants were determined by following the recovery of the diluted inhibited enzyme at room temperature (*Figures 2, S3*) and are presented in Table 4. The rates translate to half-lives that span from 13 h for dimethyl carbamate **6** and to 13 days for diethyl analogue **11**, and to Gibbs activation energies on the scale of 24–25 kcal/mol. Increasing, the size of one of the carbamate substituents to pent-4-yn-1-yl or benzyl prolonged the duration of the inhibition to approx. 2 and 4 days, respectively. The decreased steric demands and degrees of freedom in the case of dipropargyl **19** *vs*. diethyl carbamate shortened the half-lives by almost

30-fold, comparable to the dimethyl carbamate **6**. These data agree with those obtained by progress curve analysis on a same-scaffold BChEI from a previous series[52] and (with some extrapolation for different experimental conditions) the data on BChE[23] and AChE[30].
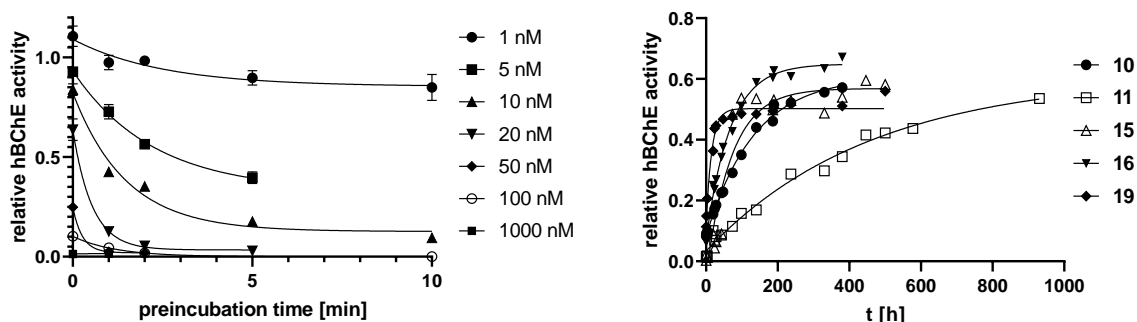
Figure 2: Left: hBChE residual activity as a function of preincubation time at different **6** concentrations. The enzyme and inhibitor were preincubated for specified lengths of time, then the substrate was added, and the initial velocities were measured and compared with the uninhibited enzyme. Values are expressed as means ± SEM of at least two duplicates. Right: reactivation of carbamoylated hBChE upon dilution for compounds **6**, **10**, **11**, **15**, **16**, **19**. The initial velocities were compared to the uninhibited, identically diluted control enzyme solution.

Table 4: Carbamoylation of hBChE by **6** and reactivation of carbamoylated hBChE – kinetic parameters.

Compound	Concentration [nM]	k_{obs} [min^{-1}]		R^2 goodness of fit
6	5	0.4475		0.9845
	10	0.6765		0.9728
	20	1.855		0.9871
	50	3.752		0.9993
	R^2 for double reciprocal plot:			0.9608
	K_i [nM]	1.05		
	k_{carb} [M^{-1} × min^{-1}]	10.635		
	k_{decarb} [h^{-1}] at 25 °C	$t_{1/2}$ [h]	Eyring $\Delta G^{\ddagger}$ [kcal/mol]	
	0.05331	13.0	24.0	0.9982
10	0.007513	92.2	25.2	0.9950
11	0.002177	318.3	25.9	0.9872
15	0.01415	49.0	24.8	0.9133
16	0.01489	46.5	24.8	0.9943
19	0.06194	11.2	24.0	0.9768

Mass spectrometry study of BChE carbamoylation

To unequivocally confirm the covalent binding of the carbamate warhead to hBChE – i.e., the carbamoylation of catalytic Ser198, we conducted a mass spectrometry study. Since the bound carbamate moiety could be hydrolysed under pepsinolytic conditions that are typically used for sample preparation for MS, whole protein mass spectrometry analysis using recombinant hBChE produced in *E. coli*[60] was undertaken. The absence of glycosylation in a protein from prokaryotic expression system was needed to produce a uniform multicharged protein spectrum. In both control and carbamoylated samples, the protein eluted at 7.2 min under our experimental conditions and the deconvolution of spectra resulted in one major species for each sample.

For **14**, the native hBChE in the control sample featured a mass of 60069 ± 1 Da (ProtParam[61] calculated mass from the primary sequence: 60069.2 Da), while the 20-min **14**-incubated sample produced a species with mass of 60183 ± 1 Da (*Figure 3*). This mass difference of 114 ± 1 Da, is in good accordance with the expected mass difference for the morpholinocarbamoylated hBChE (114.1 Da). Interestingly, injection of the same **14**-treated sample incubated for more than 60 min, showed only the presence of the free, non-carbamoylated hBChE, after deconvolution.

Similarly, for **6**, the native hBChE in the control sample featured a mass of 60073 ± 1 Da (4 Da difference to the ProtParam[61] calculated mass) and the **6**-incubated sample produced a species with mass of 60144 ± 1 Da (*Figures 3, S7*). The mass difference of 71 ± 1 Da, is in good accordance with the expected mass difference for the dimethylcarbamoylated enzyme (72.1 Da).
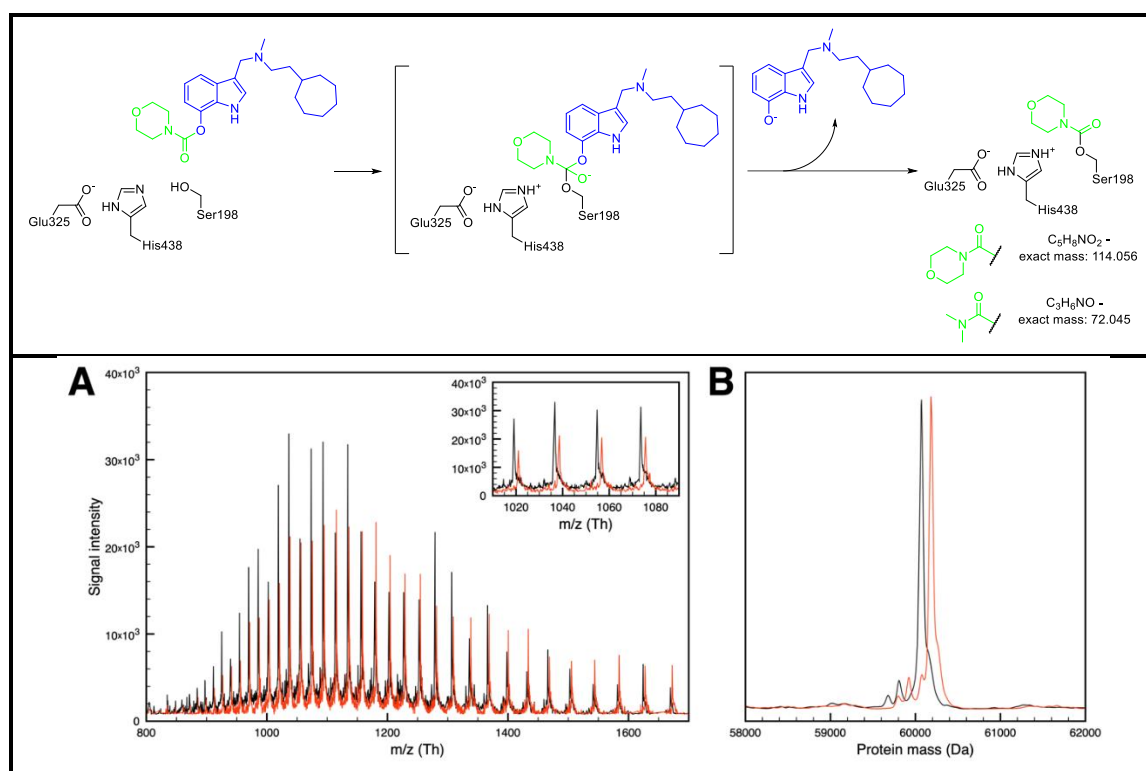
Figure 3: Above, carbamoylation of hBChE by carbamates **14** and **6**. The carbamoyl moiety is coloured green, the leaving group blue, and the enzyme black. Below, mass spectrometry analysis of hBChE carbamoylation by **14**. **A** – a characteristic protein spectra recorded at 7.2 min retention time together with a close view insert. **B** – deconvoluted spectra for control sample (black) and **14**-treated sample after 20 min (red).

Cytotoxicity

Compound **6** was also tested for cytotoxicity in the SH-SY5Y and HepG2 cell lines, with IC_{50} values of 5.8 µM and 7.1 µM, respectively (*Figure 4*). The substantial cytotoxicity of these compounds (observed at 1000-fold higher concentrations than the IC_{50}) might be the result of unspecific binding due to the high lipophilicity of the scaffold. However, this work was only meant to explore the *N*-dialkyl *O*-arylcarbamate warhead, not to produce developable lead compounds. Thus, a chosen *O*-arylcarbamate warhead can still be installed on a less cytotoxic scaffold to reap the benefits of pseudo-irreversible inhibition.
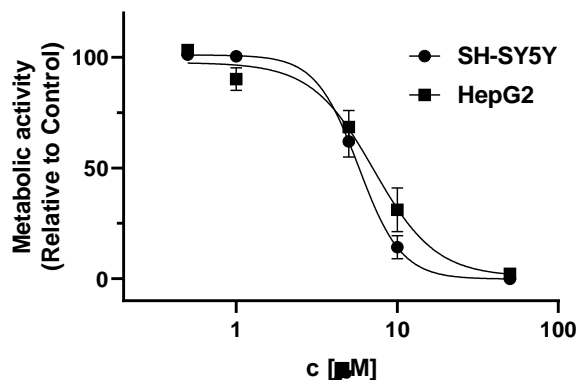
Figure 4: *In vitro* cytotoxicity profile for **6**. SH-SY5Y (●) and HepG2 (■) cells were incubated in the presence of increasing concentrations of the compounds (0.5–50 µM) in serum-reduced medium. After 48 h, the metabolic activity was evaluated using the MTS assay. The control group (DMSO) was considered as 100% cell viability. Data are means ± SEM of three independent experiments, each carried out in quadruplicate.

hBChE fluorescent labelling

Due to the brightness and excellent photostability, rhodamine B was chosen as a basis of the clickable fluorophore. Secondary amides of rhodamine B exist in a non-fluorescent spirocyclic form at neutral pH and transform into ring-opened fluorescent forms at lower pH.[62] To remove this impact of pH on the fluorescence, a ω-azido tertiary amide **26** was prepared with 1-(2-azidoethyl)piperazine, which is not prone to spirolactamisation and subsequent loss of fluorescence. Human plasma is reported to contain 3.5–9.3 mg/L (41–109 nM) BChE[2] and is therefore an excellent and readily available biological sample for labelling experiments. Three time-dependent carbamate inhibitors were chosen based on their potencies, selectivity ratios and decarbamoylation rates. The stability of carbamates in aqueous solution was also checked, and were shown to be stable for weeks under physiologically similar conditions (*Table S3*). The compounds were incubated with plasma, the whole samples were labelled using *in situ* click reaction with Cu^+ and **26**, and the mixture was resolved using SDS-PAGE, as described in the Experimental Section. The proteins were transferred to a nitrocellulose membrane using Western blotting to improve fluorescent detection. Clearly visible fluorescent bands were present only in the plasma sample treated with inhibitor **17** (*Figure 5* left, lane 4) and in the recombinant hBChE and hAChE samples labelled with **17** (*Figure 5* left, lanes 9 and 10, respectively). The labelling was abolished by preincubation with BChE-selective inhibitors ethopropazine and tetraisopropyl pyrophosphoramide (iso-OMPA; lanes 5–7) and also with AChE-selective BW284c51 (1,5-bis(4-allyldimethylammoniumphenyl)pentan-3-one dibromide; lanes 8, 11). The latter is somewhat surprising, as the reported IC_{50} for hBChE inhibition by BW284c51 is 354 µM.[63] Additional immunostaining with anti-hBChE antibodies

was performed (*Figure 5*, right), and the fluorescently labelled bands in lanes 4 and 9 were also detected by antibodies. The expected mass of fully glycosylated native plasma hBChE is 85 kDa[2,64], which agrees with the signal below the 98 kDa marker. The origins of the other fluorescent and immunostained bands are unknown; some possibilities include carbamate also binding to other serine hydrolases in plasma[65], degradation of hBChE upon storage – the so-called "storage bands"[65], and unspecific binding to human serum albumin (67 kDa). This requires further exploration, but for this proof-of-concept study, the fluorescent labelling of hBChE with clickable carbamates was confirmed.
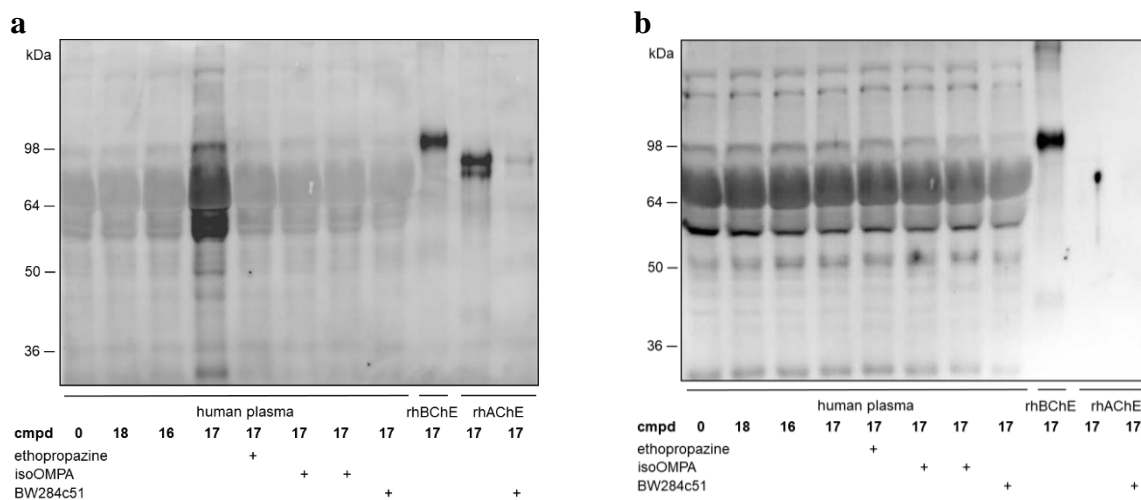
Figure 5: Western-blotted membranes after SDS-PAGE of the click-reaction-labelled samples. The samples were treated with either methanol (negative control) or 10 µM of the respective carbamate, without or with the specific hBChE inhibitor (500 µM ethopropazine, 100 µM isoOMPA), or the specific hAChE inhibitor (100 µM BW284c51). **a**, Fluorescent detection at 595 nm; **b**, Chemiluminescent detection of immunostained hBChE. For raw pictures and details of image processing procedures, see Supporting Information, Figures S4, S5.

The successful labelling only in the case of the carbamate **17** with the terminal alkyne on the longest chain (i.e., 11 carbon atoms *vs*. 3 and 5 carbon atoms for **18** and **16**, respectively) would suggest that a sufficiently long linker is required on both the side of the alkyne partner as well as the azide fluorophore, to successfully span the active site gorge and participate in the click reaction. However, this was not supported by computational studies (*vide infra*); therefore, factors other than steric limitation might be at work here. Perhaps the click reaction deeper within the active site gorge is hindered, or the leaving group **5** remains bound in the active site (as in the crystal structure; see below), to prohibit the fluorophore terminal azide from entering deep enough into the active site to reach the carbamate alkyne and for the click reaction to occur.

Furthermore, preliminary fluorescent labelling experiments in rat brain slices were undertaken. Carbamate **17** successfully blocked ChE activity, as determined by the modified Koelle−Karnovsky[48,66] histochemical method (*Figure S6*). Unfortunately, further click reaction derivatisations for labelling with the fluorophore **26** were not successful. The observed strong background fluorescence points to non-specific binding of the lipophilic fluorophore. Therefore, careful selection of the fluorophore moiety and additional optimisation are needed before this method can be applied for histochemical determination of ChEs.

Structural studies

To unambiguously confirm the covalent binding of carbamates to the catalytic serine, a potent time-dependent hBChE inhibitor **6** was selected for crystallisation. After some trial-and-error, the careful selection of the crystal soaking conditions successfully led to the crystal structure of the dimethylcarbamoylated hBChE together in complex with the leaving group **5** at a 2.14-Å resolution (PDB 8AI7, *Figure 6, left*). Continuous electron density is observed close to Ser198 and the carbamate moiety (modelled here as a dimethylformamide molecule) can be fitted with a Ser198-*O*γ DMF-carbon distance of 1.4 Å, in accordance with the formation of a covalent bond. While there are some similarities in the binding modes of the compounds from the previous series[52] – i.e., the cation-π interaction of the central tertiary amine of the leaving group with Tyr332, and a hydrophobic region above Trp82 in the choline-binding pocket that is occupied by the cycloheptyl ring – the indole moiety is this time predominantly facing the solvent (*Figure 6, right*). The reason for this is probably the steric hindrance with the dimethylcarbamoylated Ser198, where the methyl substituents encroach into the acyl-binding pocket that was previously occupied by a heterocyclic ring. The carbamoyl oxygen is nicely situated within the oxyanion hole, forming all three available hydrogen bonds with the backbone amide hydrogens of Gly116, Gly117 and Ala199. A water molecule (water 188) is located below His438 (modelled as protonated) and only 3.1 Å away from the carbonyl carbon of the dimethylcarbamate moiety, which is appropriately positioned to affect the hydrolysis and regeneration of the catalytic residue.
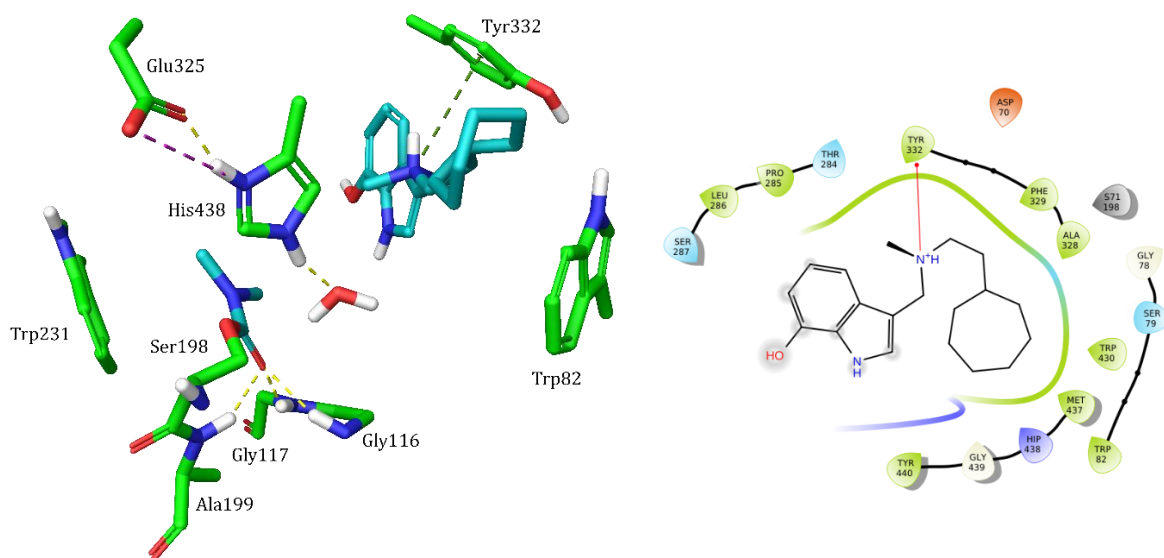
Figure 6: *Left*: Crystal structure of **5** in complex with dimethylcarbamoylated human BChE (PDB: 8AI7). The key amino acid residues are shown as green sticks, while the **5** leaving group and dimethylcarbamoyl moiety on Ser198 are teal-coloured. The hydrogen bonds are shown as yellow dashed lines, cation-π interaction with Tyr332 as dark green dashed line, and the salt bridge within the triad with magenta dashed line. Crystal water 188 is located 3.1 Å from the carbonyl carbon in an appropriate position to hydrolyse the carbamoylated catalytic Ser198. *Right:* Ligand interaction diagram for the **5** leaving group in the carbamoylated hBChE active site. The cation-π interaction of the central tertiary amine with Tyr332 is shown as a red line. The cycloheptyl still occupies the hydrophobic region above Trp82 in the choline-binding pocket, while the indole was displaced from the acyl-binding pocket and is predominantly facing the solvent (grey circles – solvent exposure).

Computational studies

To further study the binding properties and discern differential steric effects across the series of compounds, only the 7-substituted indolyl carbamates were studied *in silico*. To generate non-covalent docking poses that were in line with the known SARs, as well as the available structural data on this series of ligands (e.g., the crystal position of the cycloheptyl ring), several constraints had to be introduced (see Experimental Section); finally, two predominant binding modes were identified (cases *A* and *B*).

In case *A*, the poses obtained had carbamate alkyls oriented towards the acyl-binding pocket, while in case *B*, the poses obtained had carbamate alkyls oriented towards the choline-binding pocket (*Figure 7*). To decide which solution was more probable, binding pose metadynamics (*Figure S8*) and 1 μs all-atom molecular dynamics (MD) simulations were performed for both cases. The metadynamics suggested that case *A* pose is more stable; however, extended MD simulations revealed that both poses were unstable, as evident from the observed RMSD increase, broken hydrogen bonds with oxyanion hole residues, and the disruption of the catalytic triad (*Figure 8A–F*). Namely, visual inspection revealed that in both cases, the carbonyl of the carbamate moiety that had resided in the oxyanion hole underwent a 180 ° rotation (after 50 and 250 ns, respectively), and that the molecule distanced itself from the catalytic Ser198, thus preventing a covalent reaction. This instability of the prereaction poses suggests that this ligand does not favour the short-lived non-covalent position, consistent with the experimentally observed non-covalent inhibition for this compound. It should be however noted that other factors, such as small changes in the protonation pattern of the charged binding site residues, the force field parameters used and the use of the docking approach (which was optimised for non-covalent binding avoiding steric conflicts) might also be important for the observed outcomes.

A   **B**
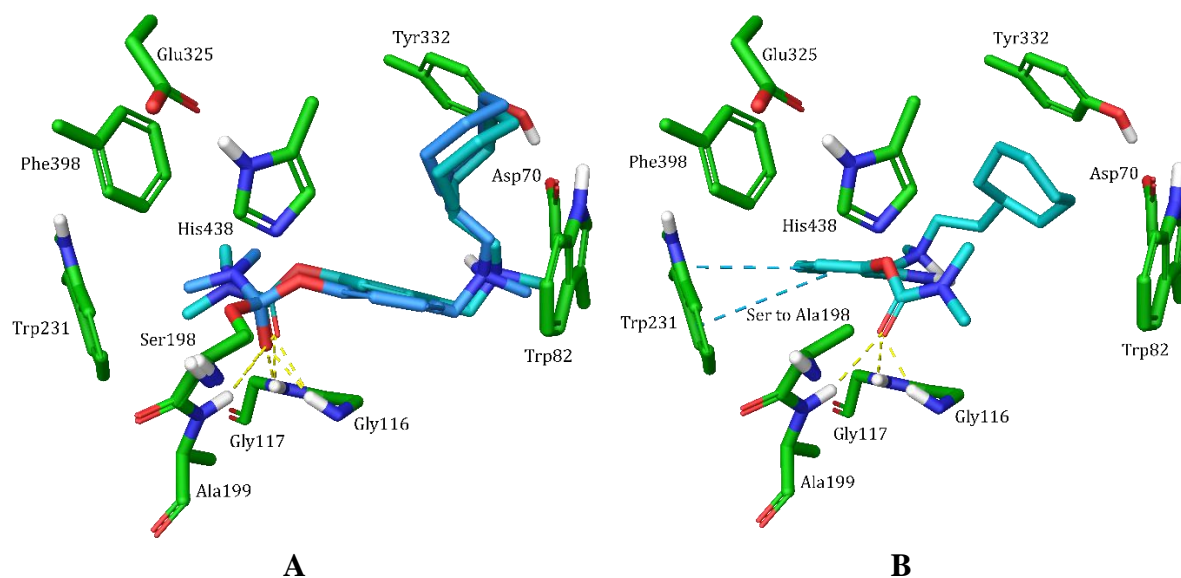
Figure 7: The two determined docking poses of compound **6** in the hBChE active site. **A**, Overlay of the prereaction (azure sticks) and postreaction (teal sticks) poses for case *A*. B, The prereaction (teal sticks) pose for case *B*. The distances between the (ex-)carbonyl carbon and *O*γ-Ser198 was 2.4 and 1.4 Å for prereaction and postreaction pose in case *A*, and 2.8 Å for prereaction pose in case *B*, respectively.
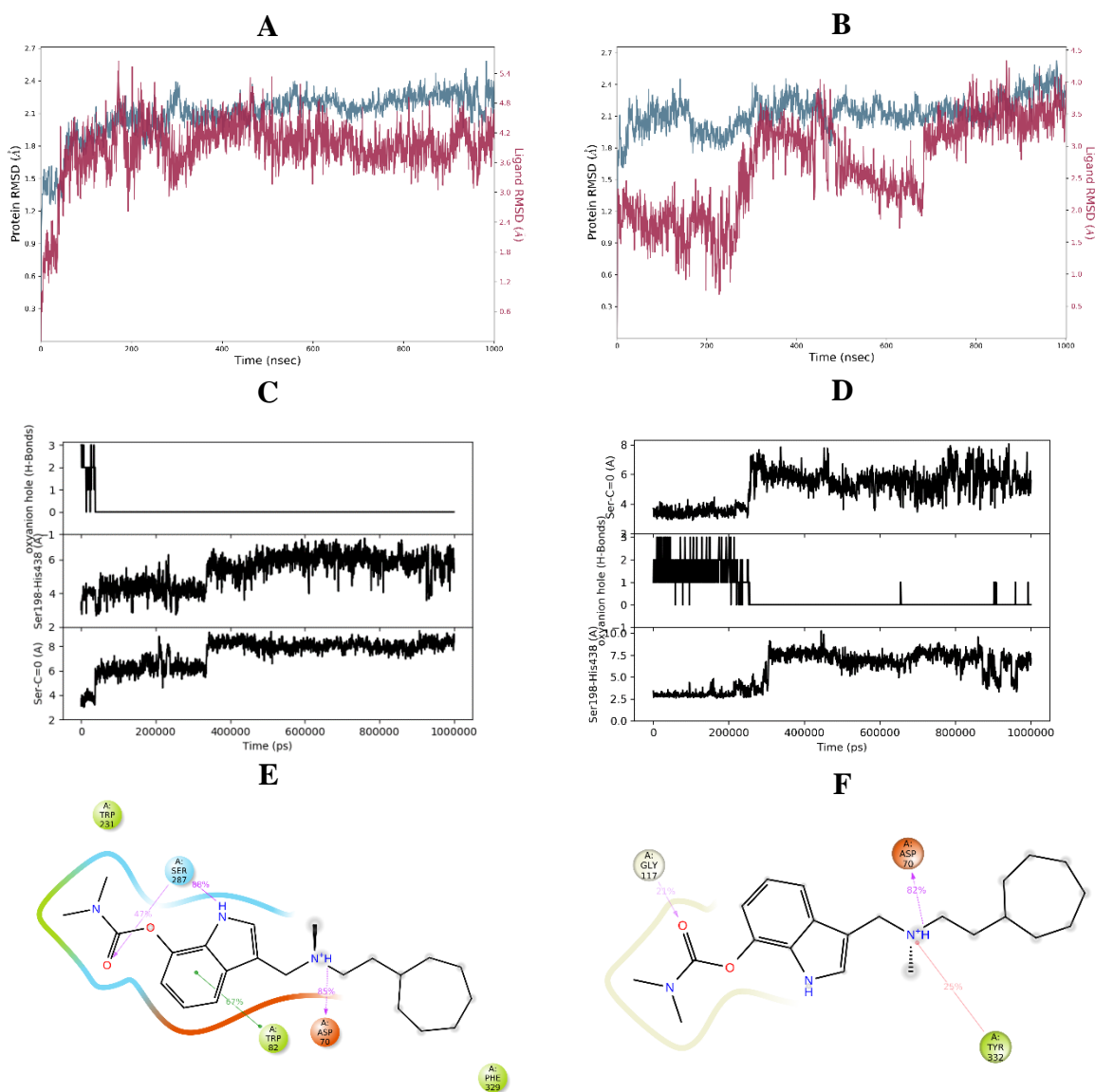
Figure 8A: Results of 1 µs all-atom MD simulations of the non-covalent prereaction docking poses of compound **6**. Left column – case *A*; and right column – case *B*. The first row (**A**, **B**) shows the RMSD plots over simulation time – the teal-coloured plot corresponds to the hBChE Cα RMSD and the red-coloured to ligand RMSD. For calculation of both parameters, all frames were first aligned to the backbone in the first, reference frame. The second row (**C**, **D**) depicts the number of hydrogen bonds formed with the oxyanion hole residues (Gly116, Gly117, Ala199), the distance between Ser198 *O*γ and His438 *N*ε (in Å, indicating the stability of the triad), and the distance between Ser198 *O*γ and **6** carbonyl carbon (in Å, indicating the propensity for covalent bond formation). The third row (**E**, **F**) shows protein-ligand contacts and interactions that occur for more than 20% of the MD simulation time. The π–π interactions are shown as green lines, the cation–π interactions as red lines, hydrogen bonds are shown in blue and ionic interactions in magenta. Both poses are unstable in the long term, as seen from the RMSD increase, broken hydrogen bonds with the oxyanion hole residues, and disruption of the catalytic triad. Visual inspection shows that in both cases the carbonyl of the carbamate moiety that resided in the oxyanion hole underwent 180 ° rotation (after 50 and 250 ns,

respectively) and that the molecule distanced itself from catalytic Ser198, preventing a covalent reaction.

Subsequently, we performed covalent docking calculations for compound **6**. Here, the observed poses appeared to favour the orientation of the carbamate alkyls towards the acyl-binding pocket (case *A*) exclusively. To provide insight into their stability, covalently bound postreaction poses from cases *A* and *B* (the latter was manually generated) were evaluated in MD simulations. As seen from Figure **9A–F**, the case *A* pose was substantially more stable, as reflected in lower RMSD, persistent three hydrogen bonds of **6** with oxyanion hole residues, stable catalytic triad (Ser198 $O\gamma$–His438 $N\varepsilon$ distance approx. 3.3 Å), and overall, more interactions formed between ligand **6** and the binding site.
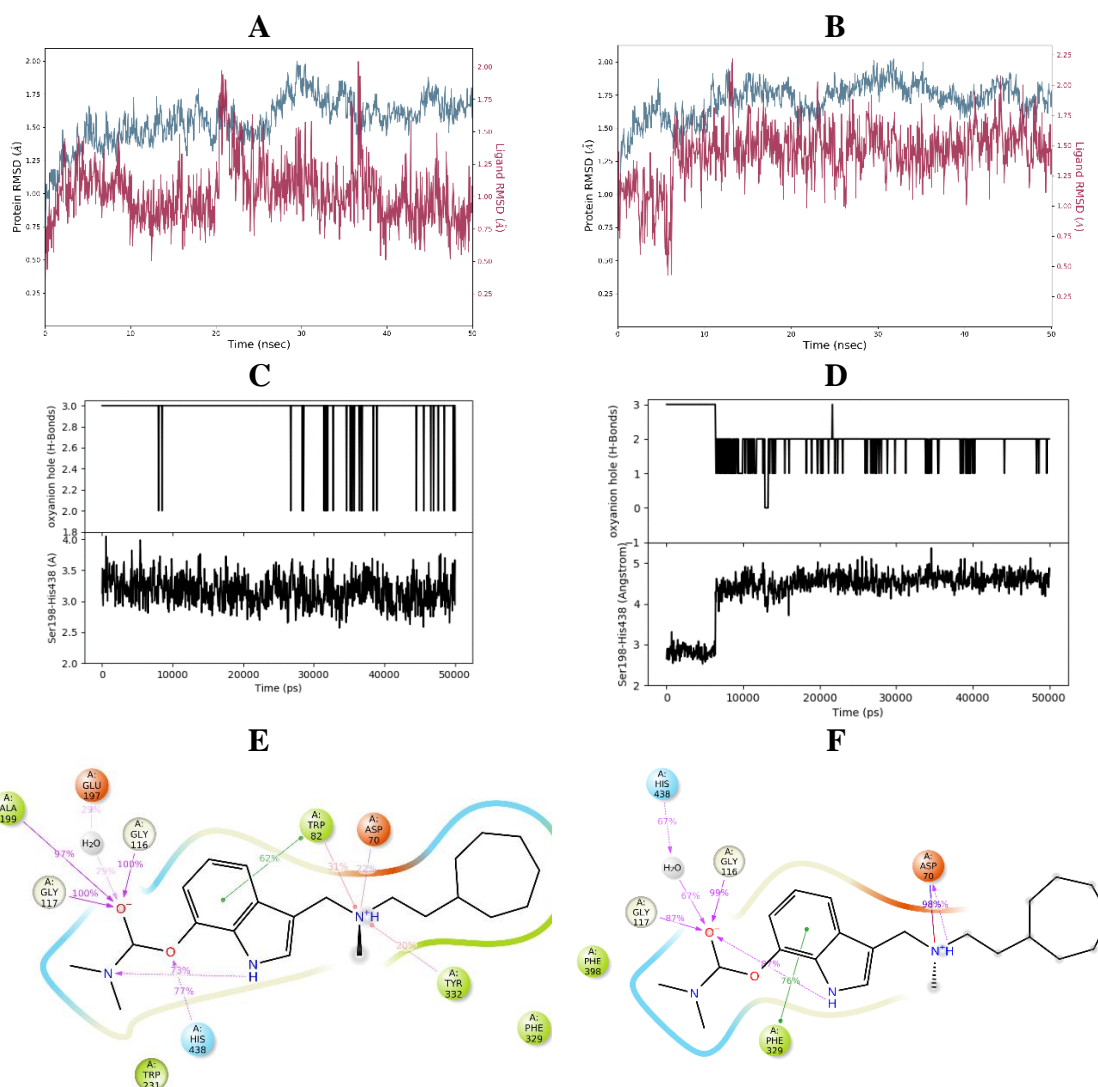
Figure 9: Results from the MD simulation of the tetrahedral intermediate formed after the nucleophilic addition of Ser198 to the **6** carbamate carbonyl. Left: a case *A* pose obtained with the CovDock covalent docking protocol; Right: a case *B* pose that was manually prepared from a Glide pose where carbamate alkyls were oriented towards the choline-binding pocket. See Figure 8 for more detailed legend.

The results of the *in silico* covalent and non-covalent binding experiments indicated that the bound orientation described by case *A* (where the carbamate alkyl is oriented towards the acyl-binding pocket) is more probable for this series of compounds. Consequently, all of the remaining 7-substituted indolyl carbamates were modelled in this way. From the pool of non-

covalently docked molecules of this series, only **9**, **12**, **18** and **20** with bulkier *N*-dialkyl substituents on the carbamate warhead produced no successful prereaction docking poses. Apart from **18**, these compounds showed time-independent profiles of reactivity in the *in vitro* assay, suggesting reversible binding only, which is in agreement with the docking results. Furthermore, the covalent docking protocol successfully produced postreaction poses for all compounds except **12** and **20**, both with bulky carbamate warheads and exhibiting time-independent behaviour in the *in vitro* assay. The analysis of MD simulations of postreaction poses for time-independent, reversible **9** (*Figure S9*) showed that both poses were comparably stable within the given timeframe and exhibited a similar interaction profile.

In case of the fluorescent labelling of hBChE with alkyne-functionalised carbamate and azide-functionalised fluorophore, the covalent docking protocol successfully docked the product of the click reaction between *N*-methyl-*N*-undec-10-yn-1-yl carbamate of compound **17** and fluorophore **26**. Additional 50 ns MD has revealed that the carbonyl oxygen remained bidentately fixed in the oxyanion hole, the long carbon atom linker spanned the active site gorge, while the bulky rhodamine B moiety remained near the entrance to the active site, exposed to the solvent, and only transiently interacted with Asp70 and Tyr332 at the peripheral site. The shorter three and five carbon atom analogues **15** and **16** also produced successful docking poses, indicating that the bulky rhodamine B fluorophore moiety of their respective click reaction products could also fit within the active site gorge (data not shown).

Altogether, the results of this computational work indicate that the steric factors in the prereaction pose have a major role in determining reactivity, as the postreaction poses fitted the active site nicely, regardless of the carbamate *N*-alkyls orientation. Furthermore, the serious steric clash that prevents the carbamoylation of Ser198 was possible to predict using different docking techniques.

To gain further insight into the intrinsic chemical reactivity of the carbamate warhead and the electronic factors that govern the carbamoylation step, we used quantum mechanical (QM) calculations to model the hydrolysis of **6** with a model nucleophile in solution. The investigated model reaction is outlined in Scheme 5: minimal representative structure, i.e., the fragment **6a** was used to reduce the size of the system, and methoxide as Ser198 surrogate. At the M06-2X/aug-cc-pVTZ(-f)//M06-2X/6-31G**++ level of theory density functional theory (DFT)-predicted Gibbs activation free energy barrier $\Delta G^{\ddagger}$ was 20.9 kcal/mol. The reaction free energy up to the tetrahedral intermediate **6d** was 14.6 kcal/mol, while the corresponding energy for the complete reaction (**6a**+**6b** to **6e**+**6f**) was exothermic, −16.4 kcal/mol (*Table S2*). This reaction was modelled in implicit water solution without taking the enzymatic environment into account, which could be better described by QM/MM techniques. Even considering the inaccuracies connected with the DFT method, and that by definition the enzymes lower the reaction barrier, typically by stabilising the transition state, the obtained reaction barrier was found to be in the same range as the experimentally determined Gibbs free energy of activation for **6**: 18.5 kcal/mol.
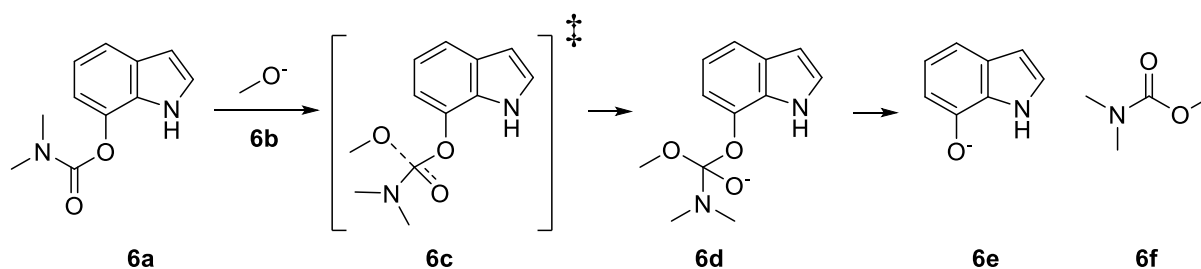
Scheme 5: The studied model reaction of **6a** with methoxide.

Altogether, these data suggest that the crucial factors that dictate the covalent mechanism of action within this series of carbamate ChEIs are the size and bulkiness of the carbamate *N*-dialkyl substituents. Significant steric clash prevents the approach to the catalytic Ser198, and efficient binding and activation by the oxyanion hole. The intrinsic reactivity of the warhead itself should be approximately the same for different carbamate *N*-dialkyl substituents and was found to be energetically comparable with the behaviour observed in solution.

Conclusion

In this work, we followed up on a series of pseudo-irreversible covalent carbamate hBChE inhibitors, and determined the carbamate warhead SARs and steric requirements/constraints for the carbamoylation of the catalytic Ser198 with dialkylcarbamoyl moieties. The covalent mechanism of binding was sequentially confirmed by IC_{50} time-dependency profiles, kinetic analysis through k_{obs} determination and recovery-upon-dilution experiments, LC-MS, and finally by X-ray crystal structure determination. For the selected 7-substituted carbamate inhibitor **6**, the mass increase corresponding to the dimethylcarbamoyl moiety was observed in whole protein LC-MS experiment, and the crystal structure of dimethylcarbamoylated enzyme together in complex with the leaving group **5** was obtained – making this the first known crystal structure of the dimethylcarbamoylated BChE.

The computational studies provided valuable insight into the steric constraints and also tentatively identified the problematic, bulky carbamate warheads that could not reach and carbamoylate the catalytic Ser198. Additionally, the determined carbamoylation rate and Gibbs free energy of activation for inhibitor **6** agreed nicely with the quantum-mechanically predicted reaction barrier for a reaction with a model nucleophile in solution. Therefore, the steric effects appear to be the crucial factors in determining the covalent binding behaviour of these carbamate ChEIs. These results bring together the missing (and in our opinion, final) pieces to the puzzle on carbamate ChEI and when translated across different scaffolds, they could aid other researchers in the selection of the correct carbamate structure to achieve the desired, prolonged duration of action.

Furthermore, the introduction of a clickable terminal alkyne moiety into one of the carbamate substituents and *in situ* derivatisation with an azide-containing fluorophore enabled fluorescent labelling of the enzyme, as was confirmed by the proof-of-concept study with plasma hBChE. This highlights the potential of this novel approach and these compounds to be developed as clickable molecular probes for investigating tissue localisation and activity of ChEs.

Experimental
Inhibition of Cholinesterases

The inhibitory potencies of the compounds against the ChEs were determined using the method of Ellman following the procedure described previously.[21] Briefly, compound stock solutions in DMSO were incubated with Ellman's reagent and the ChEs (final concentrations: 370 μM Ellman's reagent, approximately 1 nM or 50 pM hBChE or hAChE, respectively) in 0.1 M sodium phosphate pH 8.0 for 5 min at 20 °C. For time-dependency measurements, the pre-incubation time was varied (1 min, 5 min, 15 min, 30 min or 60 min). The reactions were started by the addition of the substrate (final concentration, 500 μM butyrylthiocholine iodide or acetylthiocholine iodide for hBChE and hAChE, respectively). The final content of DMSO was always 1%. The increase in absorbance at 412 nm was monitored for 2 min using a 96-well microplate reader (Synergy HT, BioTek Instruments, VT, USA). The initial velocities in the presence (v_i) and absence (v_o) of the test compounds were calculated. The inhibitory potencies were expressed as the residual activities, according to RA $= (v_i - b) / (v_o - b)$, where *b* is the

blank value using phosphate buffer without ChEs. For IC_{50} determinations, at least seven different concentrations for each compound were used. The IC_{50} values were obtained by plotting the residual ChE activities against the applied inhibitor concentrations, with the experimental data fitted to a four-parameter logistic function (GraphPad Prism 9.4). Tacrine and donepezil were used as positive controls. The progress curves for the time courses of product formation for the hydrolysis of butyrylthiocholine were measured on an Agilent Cary 3500 UV-VIS spectrophotometer with Compact Peltier (thermostatted at 25 °C) at 412 nm using a 0.6 mL 0.5 cm cuvette. 30 mM Tris buffer pH 7.0 with 1 mg/mL BSA and 0.02% NaN_3 was used and all dilutions were done in glass vessels (note: dilute hBChE solutions rapidly lose activity, presumably due to adsorption to plastic, preventing meaningful decarbamoylation assays. In our hands, under the above conditions only, the diluted and stock solutions of hBChE were stable for at least a month at room temperature.). Total volume in the cuvette was always 500 µL, and enzyme solutions that gave upon dilution $v_0 = (dA/dt) \approx 0.5$ (for carbamoylation) and ≈ 1 for (for decarbamoylation) were used. For carbamoylation experiments, 0.5–1 µL of enzyme stock, 5 µL of compound solution, and 484 µL of buffer were preincubated for the specified time, then 10 µL of the mixture of 25 mM Ellman's reagent (DTNB) and 20 mM butyrylthiocholine (large excess to prevent substrate depletion) were added, quickly mixed, and measurement started. For decarbamoylation experiments, 50 µL of the enzyme stock solution and 0.25–0.5 µL of the compound solution in MeOH (concentration chosen to achieve 85–95% inhibition, typically 0.5–1 mM) were incubated for 1 h at room temperature, then the mixture was diluted 1:1000 with the buffer, and 500 µL aliquots were drawn at different timepoint, mixed with 10 µL of the mixture of 25 mM Ellman's reagent (DTNB) and 20 mM butyrylthiocholine, and hBChE activity assayed. The data analysis followed the literature.[23,29] Experimental Gibbs free energy activation barrier $\Delta G^{\ddagger}$ was calculated from the (de)carbamoylation rates *via* the Eyring equation (taking reference concentration of 1 M, at 298.15 K).

Cytotoxicity

The human neuroblastoma SH-SY5Y and human liver carcinoma HepG2 cell lines were purchased from American Type Culture Collection (Manassas, VA, USA). Cells were cultured in Advanced Dulbecco's modified Eagle's medium (Gibco, Thermo Fisher Scientific, Waltham, MA, USA) supplemented with 10% fetal bovine serum (FBS, Gibco), 2 mM L-glutamine, 50 U/mL penicillin and 50 µg/mL streptomycin (Sigma, St. Louis, MO, USA) in a humidified atmosphere of 95% air and 5% CO_2 at 37 °C, and grown to 80% confluence. Prior to cell treatment, complete medium was replaced with serum-reduced medium (*i.e.*, with 2% FBS). **6** was prepared as a 20 mM stock solution in DMSO. The cells were seeded in 96-well plates (2 $\times 10^4$/well) and assessed by MTS ([3-(4,5-dimethylthiazol-2-yl)-5-(3-carboxymethoxyphenyl)-2-(4-sulfophenyl)-2*H*-tetrazolium, inner salt) assay for their response to **6**. Cells were treated with increasing concentrations of compounds (0.5–50 µM) in serum-reduced medium, and metabolic activity was assessed after 48 h using the CellTiter 96® Aqueous One Solution Cell Proliferation Assay (Promega, Madison, WI, USA), in accordance with the manufacturer's instructions. Absorbance was measured with an automatic microplate reader (Tecan Safire[2], Switzerland) at a wavelength of 492 nm. Results are expressed as a percentage of the control (DMSO), and are representative of three independent experiments, each performed in quadruplicate, presented as means ± SEM.

hBChE fluorescent labelling

EDTA-plasma was obtained from the author and refrigerated at 4 °C until use. Inhibitor stock solutions were prepared in MeOH. To 50 µL of plasma, 0.5 µL of 1 mM carbamate were added, giving final concentration of 10 µM, vortexed, and incubated for 30 min at room temperature.

For BChE/AChE-selective inhibitor controls, 50 µL aliquots of plasma were preincubated for 10 min with 0.5 µL of the respective inhibitor stock solution, giving final concentration of 500 µM ethopropazine, 100 µM isoOMPA, or 100 µM BW284c51, respectively, then the carbamate was added and the sample incubated for 30 min at room temperature. Recombinant hBChE and hAChE were diluted with PBS to 0.5 mg/mL and 50 µL aliquots were used as described for plasma. The click reaction followed a reported protocol.[67] Briefly, the samples were then diluted with 400 µL PBS and the following reagents were added, vortexing after each addition: 2.5 µL of 20 mM rhodamine-azide **26** in DMSO, 2.5 µL of 200 mM TCEP in water, 42.5 µL of 1.2 mM TBTA in *tert*-butanol, 2.5 µL of 200 mM aqueous copper (II) sulphate, and left at room temperature for 4 h. 5 µL of the sample solution were then added to 25 µL of water and 6 µL of the 6× loading buffer (125 mM Tris pH 6.8, 20% glycerol, 4% SDS, 0.005% bromophenol blue), thoroughly vortexed, and incubated for 5 min at 100 °C before loading onto the gel. Polyacrylamide gels were prepared in the following way: 12% acrylamide separating gel (375 mM Tris pH 8.8, 0.125% SDS, 0.125% ammonium persulphate, 425 ppm TEMED) was poured into 1.5 mm casting molds (8 mL/mold, Mini-PROTEAN®, BioRad, Hercules, CA, USA), covered with 1 mL of isopropanol, and left to polymerise for 25 min, then 15-well comb was inserted, covered with 5% acrylamide stacking gel (375 mM Tris pH 6.8, 0.1% SDS, 0.1% ammonium persulphate, 1000 ppm TEMED), and left to polymerise for 25 min. 30 µL of samples and protein standard ladder (SeeBlue™ Plus2 Pre-stained Protein Standard, Invitrogen) were loaded into the wells and the electrophoresis was run at 100 V for 2 h at room temperature in a Mini-PROTEAN® Tetra cell (BioRad, Hercules, CA, USA) filled with SDS-PAGE buffer (24 mM Tris, 192 mM glycine, 0.1% SDS). The proteins were then transferred onto a nitrocellulose membrane using a dry Western blot system (iBlot 2 Dry Blotting System, Thermo Fischer Scientific). Fluorescence was observed under epi green illumination (15 s exposure) and a 595 nm filter in a fluorescent imager (Uvitec Cambridge Alliance 9.7, Uvitec, Lodi, NJ, USA). For immunodetection of hBChE, the membranes were first incubated in 5% non-fat dry milk in TTBS buffer (25 mM Tris pH 7.4, 137 mM NaCl, 3 mM KCl, 0.1% Tween 20) for 1 h at room temperature. The membranes were washed thrice with TTBS buffer for 5 min at room temperature, followed by a 12 h incubation at 4 °C in the primary antibody solution (1:500 rabbit anti-hBChE antibody ab236577, Abcam, in 3% BSA in TTBS). The membranes were then washed thrice with TTBS buffer for 5 min at room temperature and incubated in the secondary antibody solution (1:5000 goat anti-rabbit IgG-HRP conjugate, Jackson ImmunoResearch 111-035-045, in 5% milk in TTBS) for 1 h at room temperature. The membranes were finally washed six times with TTBS buffer for 5 min at room temperature and exposed for 5 min to 700 µL of the chemiluminescent reagent (SuperSignal™ West Femto Maximum Sensitivity Substrate, Thermo Fisher Scientific). Chemiluminescence was observed in an imaging device (G-box, Syngene) in the dark.

The histochemical staining for BChE activity in coronal cryosections (10 µm) of a rat brain at the level of the thalamus followed the previously reported procedure.[68]

Crystallisation

Recombinant hBChE was produced in Chinese hamster ovary cells in a form devoid of its C-terminal end and where four residues were engineered to reduce *N*-glycosylation, as described previously.[69] Protein was purified with an initial BChE-specific affinity chromatography (Hupresin, CHEMFORASE, Rouen, France), followed by polishing and desalting with size exclusion (Superdex 200, GE Healthcare) chromatography.[70] hBChE crystals were obtained using the hanging drop method at 293 K using a 10 mg/mL protein solution and 0.1 M MES pH 6.5, 2.15 M $(NH_4)_2SO_4$ as crystallisation buffer. Stock solution of **6** (0.1 M) was prepared in 100% MeOH and the complex with hBChE was obtained by crystal soaking in 2 mM final

ligand concentration in crystallisation buffer. Crystals were cryo-protected in a solution of 0.1 M MES pH 6.5, 2.15 M $(NH_4)_2SO_4$, 20% glycerol, 1 mM ligand, 1% MeOH before flash cooling into liquid nitrogen.

X-ray Structure Determination

X-ray diffraction data were collected at the European Synchrotron Research Facility (ESRF; Grenoble, France) on the ID23-1 beamline at 100 K and images recorded on a Pilatus 6M detector (Dectris). Images were processed using the automatic data processing pipeline (GrenADES) based on XDS[71] for indexing, scaling, etc. Data analysis was realized using the Phenix software suite.[72] The structure of hBChE (PDB 1P0I) devoid of any ligand, glycan, or water molecules was used to determine the initial model by molecular replacement. Electron densities were observed in the active site gorge and allowed fitting of ligand. Ligand geometry restraints for the leaving group were processed using Phenix eLBOW[73] and the semi-empirical quantum mechanical method (AM1). Each model was refined by iterative cycles of Phenix.refine and model building using *Coot* (*Table S1*).[74] Restraints for bond formation, angles and dihedrals were applied to account for the carbamoylation of Ser198. Human BChE structure, dimethylcarbamoylated at Ser198 and in complex with **5** (leaving group of **6**), was deposited into the Protein Data Bank under accession number 8AI7.

Mass spectrometry study on whole BChE

The unglycosylated recombinant hBChE produced in *E. coli*[60] was diluted to 5 µM in MQ water, and 100 mM compound stock solutions in MeOH were further diluted with MQ water to the final concentration. The enzyme was incubated with 10 molar equivalents of the carbamate (50 µM) **6** and **14** for 5 and 20 minutes, respectively, while a non-treated aliquot served as control. Analysis was done on an Agilent 1290 Infinity UHPLC system coupled to an Agilent iFunnel Q-TOF 6550 HRMS with the following conditions: Phenomenex bioZen[TM] Intact XB-C8 LC 3.6 µm, 100 × 2.1 mm column, injection volume: 2 µL, mobile phase A: 0.1% HCOOH in ultrapure water, mobile phase B: 0.1% HCOOH in MeCN, flow: 0.4 mL/min, gradient elution: 0–2 min, 5% B; 2–16 min, 5%–100% B; 16–18 min, 100% B; 18–30 min; 5% B. The LC/MS data collected in the positive mode were treated using OpenChrom® software[75] (v 1.4) and extracted spectra were deconvoluted with UniDec software[76] (v 5.0.1).

Computational studies

Computational experiments were performed on workstations at the Department of Pharmaceutical Chemistry, Faculty of Pharmacy, and facilities of the Ažman Computing Centre at National Institute of Chemistry in Ljubljana, using Schrödinger Small Molecule Discovery Suite Release 2021-1 (Schrödinger, LLC, New York, USA, 2021) and Desmond/Maestro Non-commercial Distribution (Desmond v6.5, D. E. Shaw Research, New York, NY, USA, 2021).[77] The 6QAA and 8AI7 crystal structures were prepared using Protein Preparation Wizard: bond orders were assigned using CCD database, missing hydrogens were added, disulfide bonds were created, termini were capped, the missing side chains and loops were modelled with Prime, and het protonation states (pH 7.0 ± 2.0) were modelled with Epik[78]. All hets and cosolvent molecules except the co-crystallised ligands were removed. The crystal waters were retained. Hydrogen bonds were automatically assigned and optimised using PROPKA[79] (pH 7.0).

Non-covalent Molecular Docking
For non-covalent docking calculations, 6QAA hBChE crystal structure (resolution 1.9 Å) that was prepared as described above was used. Chain A with the co-crystallised ligand was retained while all other ligands and water molecules were removed, and Ser198 was mutated to Ala198. Receptor grid was then generated with van der Waals radii scaling by 1, partial charge cutoff

was set to 0.25, and halogens were enabled as donors. The active site was defined as the centroid of the co-crystallised ligand with innerbox of 10 $\mathring{A}^3$ and outerbox of 24.076 $\mathring{A}^3$. OPLS_2005 forcefield[80,81] was used and amide nitrogens of Gly116, Gly117, and Ala199 were defined as hydrogen donors. Ligand structures were prepared with LigPrep and ionised with Epik[78] (pH 7 ± 2) using OPLS4 force field – based on the known SAR, only the structures with ionised central tertiary amine were retained. Docking was performed using Glide XP[82] with the following modifications of the default settings: intramolecular hydrogen bonds were rewarded, a constraint of at least one hydrogen bond formed as defined in the grid with an oxygen-based acceptor was introduced, and a maximum of 3 $\mathring{A}$ RMSD of the cycloheptyl ring in the docked poses (defined by C1CCCCCC1) *vs.* its position in the 6QAA cognate ligand. This led to poses that had carbamate alkyls oriented towards the acyl-binding pocket (case *A*). Additionally, another set of non-covalent docking conditions was used (case *B*): intramolecular hydrogen bonds were rewarded, a constraint of at least one hydrogen bond formed as defined in the grid with an oxygen-based acceptor was introduced, and a maximum of 1 $\mathring{A}$ RMSD of the indole ring in the docked poses (defined by RMSD subset atoms) *vs.* its position in the 6QAA cognate ligand. This approach led to poses that had carbamate alkyls oriented towards the choline-binding pocket (case *B*). The output poses were visualised with Maestro.

Covalent Molecular Docking

The CovDock protocol[83] was used for covalent docking of the carbamate ligands and the fluorophore-labelled products of the click reaction. We again used the prepared 6QAA crystal structure, His438 residue was manually modified to charged HIP438 to ensure the proper postreaction structure, and Ser198 was negatively ionised. Ser198 was selected as the reactive residue, the box was defined as the centroid of the co-crystallised ligand in 6QAA with the size defined by the ligand. Reaction type was customised using a custom chemistry file (see Supporting Information) to correctly produce a negatively charged tetrahedral intermediate, since the default nucleophilic addition to a double bond led to a neutral one. No constraints were imposed and the thorough pose prediction docking mode was used. The results were visualised in Maestro and the obtained docking poses with cycloheptyl ring outside its well-defined position above Trp82 (*vide supra*) or with the ex-carbonyl anionic oxygen located outside the oxyanion hole were removed. The remaining poses were ranked by score and favourable interactions with the peripheral site residues (Tyr332, Asp70). For the case *B* poses, the prereaction poses from non-covalent docking were manually modified (bond formed between the carbonyl carbon and $O\gamma$-Ser198, and its length set to optimal, His438 protonated on $N\varepsilon$, double bond of the carbonyl changed to single, and carbonyl oxygen negatively charged) to produce the corresponding postreaction states that were later used for MD.

Molecular Dynamics

The structures from the docking calculations were used to prepare the systems for molecular dynamics (MD) simulations with System Builder. For non-covalently docked poses, mutated Ala198 was first reverted to Ser198, then TIP4P[84] water molecules were added up to 10 $\mathring{A}$ from the protein surface to solvate the protein in a orthorombic box. Next, Na^+ and Cl^- ions were added to neutralise the system and produce the final 0.15 M concentration. OPLS_2005 force field[80,81] was used for parametrisation of the macromolecule as well as the ligand. Default Desmond relaxation protocol (desmond_npt_relax.msj) was used for the equilibration stage: (1) 100 ps of Brownian Dynamics NVT, 10 K, small timesteps, with restraints on the solute heavy atoms, (2) 12 ps NVT, 10 K, with small timesteps and restraints on the solute heavy atoms, (3) 12 ps NPT, 10 K, and restraints on the solute heavy atoms, (4) 24 ps unrestrained NPT; followed by the production stage. The following setup was used for the MD production stage: 1.2 ps interval for energy, isothermal-isobaric NPT ensemble at 300 K and 1.013 bar pressure with Langevin thermostat and barostat (1 and 2 ps relaxation time, respectively, isotropic coupling),

RESPA integrator with 2 fs time step, cut-off scheme at 9.0 Å, and random seed. The simulations times were 20–1000 ns with 1000 frames per trajectory. The simulation results were analysed using the built-in Desmond tools. In addition, the binding pose metadynamics for the compound **6** case *A* and *B* poses obtained from non-covalent docking followed the default workflow (10 simulations/pose).

Quantum Mechanical Calculations

The quantum mechanical (QM) density functional theory (DFT) calculations for the model reaction of **6a** with methoxide were carried out in Jaguar[85]. After the initial rough MacroModel minimisation, the structures were geometrically optimised at M06-2X/6-31G**++ level and solvent effects were modelled by self-consistent reaction field method using the Poisson-Boltzmann (PBF) solver in water. The structures were checked for the absence of imaginary frequencies to confirm that they correspond to geometric minima. The ultrafine pseudospectral grids were used for the geometry optimisation, followed by full analytic integrals for single point frequency calculation at M06-2X/aug-cc-pVTZ(-f) level with PBF solver in water. For anionic intermediates, the stop_rxn=3 and geoconv_mode=standard keywords had to be used to successfully model the unstable intermediates. The transition state was located using the QST (quadratic synchronous transit) method and further verified by the presence of one imaginary frequency in the direction of the reaction coordinate and by an intrinsic reaction coordinate scan (IRC) in direction of both reactants and products. The calculated total energies for reactants, intermediates, and products were compared to calculate the reaction energetics.

Chemistry – General Information

The reagents and solvents were used as received from commercial suppliers. Tetrahydrofuran (THF) was distilled from sodium/benzophenone and stored under Ar over 4 Å molecular sieves prior to use. After extraction, organic phases were dried over anhydrous sodium sulphate. Reactions were monitored using analytical thin-layer chromatography (TLC) on silica gel 60 F_{254} Al plates. Developed plates were inspected under UV light and, if necessary, visualised with ninhydrin, vanillin/sulphuric acid, Dragendorff's or potassium permanganate stains. Melting points were determined with Büchi 535 Melting Point Appartus (uncorrected). Nuclear magnetic resonance spectra were recorded on a Bruker Avance III 400 MHz spectrometer at 400 MHz for ^{1}H, 100 MHz for ^{13}C, and 376 MHz for ^{19}F nucleus, respectively, using DMSO-d_6 or $CDCl_3$ with TMS as the internal standard, as solvents. Chemical shifts are reported in *parts per million* (ppm), the central peak of the residual non-deuterated solvent signal was used as the reference, *i.e.*, for $CDCl_3$ at 7.27 ppm for ^{1}H and 77.16 ppm for ^{13}C, and for DMSO-d_6 at 2.50 ppm for ^{1}H and 39.52 ppm for [13]C. Alternatively, the TMS peak was calibrated to 0 ppm. [19]F spectra were not calibrated. The multiplicities are reported as follows: s (singlet), d (doublet), t (triplet), q (quartet), hept, (heptet), m (multiplet), dd (doublet of doublets), ddd (doublet doublet of doublets), td (triplet of doublets), qd (quartet of doublets), and br (broad), coupling constants (*J*) quoted in Hertz (Hz), number of equivalent nuclei (by integration). Mass spectra were recorded on Thermo Scientific Q Executive Plus LC-MS/MS and Advion Expression CMS mass spectrometers and IR spectra on Thermo Nicolet FT-IR spectrophotometer. Column chromatography was performed on silica gel (Silica gel 60, particle size: 0.035–0.070 mm, Merck). UPLC analyses were performed on Thermo Scientific Dionex UltiMate 3000 modular system (Thermo Fisher Scientific Inc.). The general method used a Waters Acquity UPLC® HSS C18 SB column (2.1 × 50 mm, 1.8 µm) thermostated at 40 °C, with: injection volume, 5 µL; sample, 0.1–0.2 mg/mL in MeOH; flow rate, 0.4 mL/min; detector λ, 220 and 254 nm; mobile phase A: 0.1% TFA (v/v) in water; mobile phase B: MeCN. Gradient: 0–2 min, 20% B; 2–5 min, 20%–90% B; 5–8 min, 90% B. All compounds are >95% pure by UPLC analysis.

General procedure 1 (GP1) – Mannich reaction with 2-cycloheptyl-N-methylethan-1-amine: Parent indole (1.0 mmol) was dissolved in EtOAc (1 mL), glacial AcOH (1 mL), formaldehyde (1.2 eq., 37%, 89 µL), and 2-cycloheptyl-*N*-methylethan-1-amine[86] (171 mg, 1.1 eq.) were added, and the reaction mixture was stirred at rt for 18 h. The volatile components were removed *in vacuo* and the product was purified following *GP2*.

General procedure 2 (GP2) – RP-CC purification: Compounds were purified by reversed-phase column chromatography (RP-CC) (Isolera Biotage One Flash Chromatography system, Biotage® Sfär C18 Duo 100 Å 30 µm column, 30 g) using a gradient of 0.1% TFA in deionised water and MeCN as eluent (gradient 0–100% MeCN in 6 column volumes (300 mL); 100% MeCN for 2 column volumes (100 mL)). After the RP-CC, fractions containing the product were combined and organic volatiles were evaporated *in vacuo*. The remaining aqueous solution was made alkaline (pH 10) with 1 M NaOH$_{(aq)}$ and extracted with DCM (2 × 30 mL). The combined organic phase was dried over anhydrous sodium sulphate, filtered, and volatile components evaporated *in vacuo* to afford pure product.

3-(((2-Cycloheptylethyl)(methyl)amino)methyl)-1*H*-indol-7-ol (5)

1*H*-Indol-7-ol[87] (92 mg, 0.692 mmol), TBDMSCl (1.1 eq., 114 mg), and imidazole (1.2 eq., 56 mg) in DMF (2 mL) were stirred at rt under Ar for 18 h. 7-((*Tert*-butyldimethylsilyl)oxy)-1*H*-indole[88] was isolated by column chromatography on silica (1. PE; 2. PE/DCM = 5:1). Yield: 138 mg (0.558 mmol, 80.6%). *N*-((7-((*Tert*-butyldimethylsilyl)oxy)-1*H*-indol-3-yl)methyl)-2-cycloheptyl-*N*-methylethan-1-amine was prepared following *GP1* from 7-((*tert*-butyldimethylsilyl)oxy)-1*H*-indole (124 mg, 0.5 mmol), and isolated by *GP2*. Yield: 156 mg (0.376 mmol, 75.2%) of beige semisolid. ESI-HRMS: m/z = 415.3128 (MH$^+$); C$_{25}$H$_{43}$N$_2$OSi requires: m/z = 415.3139 (MH$^+$). ν_{max} 3490, 2924, 2854, 2787, 1622, 1577, 1498, 1461, 1360, 1337, 1253, 1078, 994, 833, 781, 729, 681 cm^{-1}. ^{1}H NMR (400 MHz, CDCl$_3$) δ = 0.27 (s, 6H), 1.05 (s, 9H), 1.13 – 1.21 (m, 2H), 1.34 – 1.70 (m, 13H), 2.23 (s, 3H), 2.42 – 2.46 (m, 2H), 3.68 (s, 2H), 6.62 (d, *J*=7.4, 1H), 6.96 (t, *J*=7.8, 1H), 7.11 (d, *J*=2.0, 1H), 7.29 – 7.31 (m, 1H), 8.05 (s, 1H). ^{13}C NMR (101 MHz, CDCl$_3$) δ = –4.09, 18.37, 25.95, 26.57, 28.61, 34.90, 35.90, 37.68, 42.47, 52.97, 55.86, 110.15, 112.74, 114.17, 119.92, 123.07, 129.36, 130.05, 141.42.

N-((7-((*Tert*-butyldimethylsilyl)oxy)-1*H*-indol-3-yl)methyl)-2-cycloheptyl-*N*-methylethan-1-amine (100 mg, 0.241 mmol) and potassium bifluoride (20 eq., 376 mg) in MeOH (5 mL) were stirred at rt under Ar for 6 h. 3-(((2-Cycloheptylethyl)(methyl)amino)methyl)-1*H*-indol-7-ol was isolated following *GP2*. Yield: 42 mg (0.14 mmol, 58.0%) of brownish semisolid, unstable in air. ESI-HRMS: m/z = 301.2261 (MH$^+$); C$_{19}$H$_{29}$N$_2$O requires: m/z = 301.2274 (MH$^+$). ν_{max} 2919, 2850, 1673, 1577, 1442, 1361, 1249, 1099, 1050, 976, 787, 728 cm^{-1}. Purity: UPLC (220 nm): t_r = 4.150 min, 99.2% total area. ^{1}H NMR (400 MHz, CDCl$_3$) δ = 1.00 – 1.09 (m, 2H), 1.24 – 1.56 (m, 14H), 2.26 (s, 3H), 2.54 – 2.61 (m, 2H), 3.80 (s, 2H), 6.59 (d, *J*=7.3, 1H), 6.89 – 6.97 (m, 2H), 7.01 (d, *J*=7.9, 1H), 9.81 (br s, 1H), 10.36 (br s, 1H). ^{13}C NMR (101 MHz, CDCl$_3$) δ = 26.36, 28.51, 34.12, 34.59, 37.75, 40.72, 52.06, 55.40, 107.92, 108.73, 109.01, 120.96, 125.12, 128.11, 129.87, 145.58.

3-(((2-Cycloheptylethyl)(methyl)amino)methyl)-1*H*-indol-7-yl dimethylcarbamate (6)

7-(Benzyloxy)-1*H*-indole (500 mg, 2.24 mmol) was dissolved in EtOAc (15 mL), flushed with Ar, then 10% Pd/C (50 mg) was added, and the resulting mixture was hydrogenated at rt under H$_2$ (balloon pressure) for 24 h. The catalyst was removed by filtration, washed with EtOAc (10 mL), and the filtrate evaporated *in vacuo* to afford crude 1*H*-indol-7-ol as grayish semisolid, unstable in air. Yield: 292 mg (2.19 mmol, 97.8%).

1*H*-Indol-7-ol (150 mg, 1.13 mmol), *N*,*N*-dimethylcarbamoyl chloride (1.5 eq., 156 µL), and DIPEA (500 µL) in MeCN (3 mL) were stirred at rt under Ar for 18 h. 1*H*-Indol-7-yl dimethylcarbamate[89] was isolated by column chromatography on silica (1. PE/EtOAc = 4:1; 2. PE/EtOAc = 1:1). Yield: 69 mg (0.338 mmol, 29.9%) of beige semisolid. [Note: the *C3*-carbamoylation seems to be a competing reaction. The *O*-carbamoylated product turns red, not blue, upon spraying and heating the TLC plate with vanillin/sulphuric acid. The selective *O*-carbamoylation can be achieved by substituting DIPEA for *N*-methylimidazole – carbamoyl chloride and *N*-methylimidazole are premixed for 5 min, then indolol is added, and the mixture stirred at 80 °C for 6 h.]

ESI-HRMS: m/z = 205.0968 (MH$^+$); $C_{11}H_{13}N_2O_2$ requires: m/z = 205.0972 (MH$^+$). v_{max} 3276, 2924, 1699, 1496, 1445, 1392, 1342, 1232, 1217, 1173, 1044, 847, 783, 722 cm^{-1}. Purity: UPLC (220 nm): t_r = 3.803 min, 95.2% total area. ^{1}H NMR (400 MHz, CDCl$_3$) δ = 3.06 (s, 3H), 3.17 (s, 3H), 6.56 (dd, *J*=2.1, 3.2, 1H), 6.96 – 6.99 (m, 1H), 7.06 – 7.10 (m, 1H), 7.12 (t, *J*=2.7, 1H), 7.48 – 7.52 (m, 1H), 8.56 (br s, 1H). ^{13}C NMR (101 MHz, CDCl$_3$) δ = 36.75, 103.09, 113.78, 117.96, 119.80, 124.83, 128.57, 130.97, 137.17, 154.59.

3-(((2-Cycloheptylethyl)(methyl)amino)methyl)-1*H*-indol-7-yl dimethylcarbamate was prepared following *GP1* from 1*H*-indol-7-yl dimethylcarbamate (36 mg, 0.176 mmol). Yield: 25 mg (0.0673 mmol, 38.2%) of beige semisolid. ESI-HRMS: m/z = 372.2640 (MH$^+$); $C_{22}H_{34}N_3O_2$ requires: m/z = 372.2646 (MH$^+$). v_{max} 3298, 2917, 2850, 2784, 1714, 1699, 1449, 1394, 1349, 1224, 1174, 1048, 1026, 846, 784, 755, 734 cm^{-1}. Purity: UPLC (220 nm): t_r = 4.453 min, 99.7% total area. ^{1}H NMR (400 MHz, CDCl$_3$) δ = 1.13 – 1.22 (m, 2H), 1.35 – 1.71 (m, 13H), 2.21 (s, 3H), 2.39 – 2.44 (m, 2H), 3.05 (s, 3H), 3.17 (s, 3H), 3.67 (s, 2H), 6.94 (dd, *J*=0.7, 7.7, 1H), 7.03 – 7.09 (m, 2H), 7.53 – 7.56 (m, 1H), 8.38 (s, 1H). ^{13}C NMR (101 MHz, CDCl$_3$) δ = 26.58, 28.62, 34.92, 35.88, 36.81, 36.98, 37.73, 42.40, 52.91, 55.86, 113.86, 114.09, 116.85, 119.56, 124.12, 128.98, 131.15, 137.09, 154.56.

3-(((2-Cycloheptylethyl)(methyl)amino)methyl)-1*H*-indol-7-yl ethyl(methyl)carbamate (7)

1*H*-Indol-7-ol (181 mg, 1.36 mmol), ethylmethylcarbamoyl chloride (1.5 eq., 248 mg), and DIPEA (500 µL) in MeCN (3 mL) were stirred at rt under Ar for 18 h. 1*H*-Indol-7-yl ethyl(methyl)carbamate was isolated by column chromatography on silica (PE/EtOAc = 4:1). Yield: 102 mg (0.467 mmol, 34.4%) of beige semisolid, that was immediately used further.

3-(((2-Cycloheptylethyl)(methyl)amino)methyl)-1*H*-indol-7-yl ethyl(methyl)carbamate was prepared following *GP1* from 1*H*-indol-7-yl ethyl(methyl)carbamate (75 mg, 0.344 mmol). Yield: 65 mg (0.169 mmol, 49.0%) of brown oil. ESI-HRMS: m/z = 386.2796 (MH$^+$); $C_{23}H_{36}N_3O_2$ requires: m/z = 386.2802 (MH$^+$). v_{max} 3307, 2918, 2851, 2788, 1703, 1445, 1399, 1349, 1301, 1286, 1222, 1164, 1088, 971, 783, 756, 730 cm^{-1}. Purity: UPLC (220 nm): t_r = 4.593 min, 97.6% total area. ^{1}H NMR (400 MHz, CDCl$_3$) δ = 1.12 – 1.71 (m, 18H), 2.21 (s, 3H), 2.40 – 2.44 (m, 2H), 3.04 and 3.15 (2 × s, 3H), 3.46 and 3.55 (2 × q, *J*=7.1, 2H), 3.68 (s, 2H), 6.94 (t, *J*=7.4, 1H), 7.06 (t, *J*=7.8, 1H), 7.10 (d, *J*=2.2, 1H), 7.54 (d, *J*=7.9, 1H), 8.32 and 8.35 (2 × s, 1H). ^{13}C NMR (101 MHz, CDCl$_3$) δ = 12.65, 13.49, 26.61, 28.65, 29.85, 34.58, 34.94, 35.87, 37.75, 42.40, 44.42, 44.50, 52.90, 55.84, 113.85, 114.07, 116.81, 116.86, 119.64, 124.17, 129.01, 129.04, 131.20, 137.15, 154.13, 154.29. A mixture of conformers.

3-(((2-Cycloheptylethyl)(methyl)amino)methyl)-1*H*-indol-7-yl isopropyl(methyl)carbamate (8)

N-Isopropylmethylamine (500 µL, 4.8 mmol) and CDI (1.0 eq., 778 mg) in DCM (5 mL) were stirred at rt for 12 h. The reaction mixture was extracted with water (10 mL, discarded), dried with sodium sulphate, the solvent was removed *in vacuo*, the residue dissolved in MeCN (5 mL), iodomethane (1.2 eq., 448 µL) was added, and the mixture stirred under Ar at rt for 18h.

The solvent was removed *in vacuo*, the residue redissolved in MeCN (5 mL), 1*H*-indol-7-ol (141 mg, 1.06 mmol) and DIPEA (500 µL) were added, and the reaction mixture stirred at 60 °C for 4 h. The solvent was removed *in vacuo* and 1*H*-indol-7-yl isopropyl(methyl)carbamate isolated by column chromatography on silica (PE/EtOAc = 4:1). Yield: 193 mg (0.831 mmol, 78.4%) of pinkish solid. mp 86.5–87.2 °C. ESI-HRMS: m/z = 233.1296 (MH$^+$); $C_{13}H_{17}N_2O_2$ requires: m/z = 233.1285 (MH$^+$). ν_{max} 3317, 2981, 1686, 1495, 1437, 1397, 1335, 1229, 1214, 1119, 889, 777, 724 cm^{-1}. Purity: UPLC (254 nm): t_r = 4.647 min, 99.7% total area. ^{1}H NMR (400 MHz, CDCl$_3$) δ = 1.21 – 1.33 (m, 6H), 2.94 and 3.01 (2 x s, 3H), 4.52 – 4.68 (m, 1H), 6.57 (dd, *J*=2.1, 3.1, 1H), 6.99 (t, *J*=8.4, 1H), 7.10 (t, *J*=7.8, 1H), 7.11 – 7.17 (m, 1H), 7.51 (d, *J*=7.8, 1H), 8.47 – 8.61 (m, 1H). ^{13}C NMR (101 MHz, CDCl$_3$) δ = 19.67, 20.28, 27.84, 27.92, 47.30, 47.74, 103.06, 113.68, 117.86, 119.77, 124.77, 130.93, 137.23, 153.95. Carbamate carbons are duplicated due to two rotamer populations.

3-(((2-Cycloheptylethyl)(methyl)amino)methyl)-1*H*-indol-7-yl isopropyl(methyl)carbamate was prepared following *GP1* from 1*H*-indol-7-yl isopropyl(methyl)carbamate (133 mg, 0.573 mmol). Yield: 139 mg (0.348 mmol, 60.7%) of beige oil. ESI-HRMS: m/z = 400.2952 (MH$^+$); $C_{24}H_{38}N_3O_2$ requires: m/z = 400.2959 (MH$^+$). ν_{max} 3319, 2920, 2851, 2790, 1698, 1499, 1444, 1334, 1223, 1170, 1121, 1004, 908, 822, 755, 730 cm^{-1}. Purity: UPLC (220 nm): t_r = 4.647 min, 98.3% total area. ^{1}H NMR (400 MHz, CDCl$_3$) δ = 1.17 – 1.28 (m, 8H)f, 1.16 – 1.29 (m, 1H), 1.37 – 1.74 (m, 13H), 2.22 (s, 3H), 2.41 – 2.46 (m, 2H), 2.91 and 2.98 (2 x s, 3H), 3.68 (s, 2H), 4.49 – 4.64 (m, 1H), 6.95 (t, *J*=8.3, 1H), 7.04 (d, *J*=2.2, 1H), 7.07 (t, *J*=7.8, 1H), 7.56 (d, *J*=7.9, 1H), 8.56 and 8.63 (2 x s, 1H). ^{13}C NMR (101 MHz, CDCl$_3$) δ = 19.59, 20.21, 26.45, 27.75, 27.80, 28.49, 34.79, 35.74, 37.60, 42.22, 47.19, 47.62, 52.77, 55.71, 113.62, 113.70, 116.53, 116.61, 119.34, 124.12, 128.92, 131.02, 137.05, 153.93, 154.08. Two sets of rotamer signals.

3-(((2-Cycloheptylethyl)(methyl)amino)methyl)-1*H*-indol-7-yl *tert*-butyl(methyl)carbamate (9)

N-Methyl-*tert*-butylamine (200 µL, 1.67 mmol) and CDI (1.0 eq., 271 mg) in DCM (5 mL) were stirred at rt for 12 h. The reaction mixture was extracted with water (10 mL, discarded), dried with sodium sulphate, the solvent was removed *in vacuo*, the residue dissolved in MeCN (5 mL), iodomethane (1.2 eq., 156 µL) was added, and the mixture stirred under Ar at rt for 18 h. The solvent was removed *in vacuo*, the residue redissolved in MeCN (5 mL), 1*H*-indol-7-ol (97 mg, 0.73 mmol) and DIPEA (500 µL) were added, and the reaction mixture stirred at 60 °C for 4 h. The solvent was removed *in vacuo* and 1*H*-indol-7-yl *tert*-butyl(methyl)carbamate isolated by column chromatography on silica (PE/EtOAc = 4:1). Yield: 130 mg (0.528 mmol, 72.3%) of beige semisolid [^{1}H NMR (400 MHz, CDCl$_3$) δ = 1.55 (s, 9H), 3.17 (s, 3H), 6.59 (dd, *J*=2.1, 3.2, 1H), 7.00 (dd, *J*=0.7, 7.7, 1H), 7.11 (t, *J*=7.8, 1H), 7.14 – 7.16 (m, 1H), 7.50 – 7.53 (m, 1H), 8.46 (s, 1H). ^{13}C NMR (101 MHz, CDCl$_3$) δ = 28.67, 32.00, 56.40, 103.06, 113.83, 117.70, 119.77, 124.73, 128.72, 130.85, 137.08, 154.10.], that was immediately used further following *GP1* to afford 3-(((2-cycloheptylethyl)(methyl)amino)methyl)-1*H*-indol-7-yl *tert*-butyl(methyl)carbamate. Yield: 156 mg (0.377 mmol, 71.4%) of beige oil. ESI-HRMS: m/z = 414.3104 (MH$^+$); $C_{25}H_{40}N_3O_2$ requires: m/z = 414.3115 (MH$^+$). ν_{max} 3352, 2919, 2851, 2789, 1705, 1632, 1579, 1458, 1345, 1221, 1157, 1110, 995, 842, 757, 730 cm^{-1}. Purity: UPLC (220 nm): t_r = 4.783 min, 99.4% total area. ^{1}H NMR (400 MHz, CDCl$_3$) δ = 1.16 – 1.25 (m, 2H), 1.36 – 1.75 (m, 22H), 2.23 (s, 3H), 2.42 – 2.47 (m, 2H), 3.14 (s, 3H), 3.69 (s, 2H), 6.95 (dd, *J*=0.7, 7.7, 1H), 7.03 – 7.10 (m, 2H), 7.56 (d, *J*=7.9, 1H), 8.45 (s, 1H). ^{13}C NMR (101 MHz, CDCl$_3$) δ = 26.48, 28.52, 28.65, 31.97, 34.82, 35.78, 37.62, 42.24, 52.81, 55.72, 56.34, 113.82, 116.54, 119.41, 124.04, 129.09, 131.01, 136.94, 154.09.

3-(((2-Cycloheptylethyl)(methyl)amino)methyl)-1*H*-indol-7-yl benzyl(methyl)carbamate (10)

N-Methylbenzylamine (200 µL, 1.55 mmol) and CDI (1.0 eq., 251 mg) in DCM (5 mL) were stirred at rt for 12 h. The reaction mixture was extracted with water (10 mL, discarded), dried with sodium sulphate, the solvent was removed *in vacuo*, the residue dissolved in MeCN (5 mL), iodomethane (1.2 eq., 145 µL) was added, and the mixture stirred under Ar at rt for 18 h. The solvent was removed *in vacuo*, the residue redissolved in MeCN (5 mL), 1*H*-indol-7-ol (97 mg, 0.73 mmol) and DIPEA (500 µL) were added, and the reaction mixture stirred at 60 °C for 4 h. The solvent was removed *in vacuo* and 1*H*-indol-7-yl benzyl(methyl)carbamate isolated by column chromatography on silica (PE/EtOAc = 4:1). Yield: 168 mg (0.599 mmol, 82.1%) of beige semisolid, that was immediately used further following *GP1* to afford 3-(((2-cycloheptylethyl)(methyl)amino)methyl)-1*H*-indol-7-yl benzyl(methyl)carbamate. Yield: 221 mg (0.494 mmol, 82.4%) of beige oil. ESI-HRMS: m/z = 448.2951 (MH$^+$); $C_{28}H_{38}N_3O_2$ requires: m/z = 448.2959 (MH$^+$). v_{max} 3323, 2919, 2851, 2783, 1704, 1633, 1580, 1452, 1397, 1351, 1216, 1168, 1125, 1028, 730, 698 cm^{-1}. Purity: UPLC (220 nm): t_r = 4.820 min, 99.4% total area. ^{1}H NMR (400 MHz, CDCl$_3$) δ = 1.19 – 1.29 (m, 2H), 1.41 – 1.78 (m, 13H), 2.24 and 2.26 (2 x s, 3H), 2.44 – 2.52 (m, 2H), 3.08 and 3.10 (2 x s, 3H), 3.70 and 3.73 (2 x s, 2H), 4.58 and 4.66 (2 x s, 2H), 6.93 – 7.16 (m, 3H), 7.34 – 7.48 (m, 5H), 7.55 – 7.65 (m, 1H), 8.13 and 8.80 (2 x s, 1H). ^{13}C NMR (101 MHz, CDCl$_3$) δ = 26.42, 28.46, 34.21, 34.75, 35.55, 35.68, 37.55, 42.15, 52.71, 52.87, 53.13, 55.69, 113.61, 113.67, 113.86, 116.68, 119.27, 124.02, 124.23, 127.09, 127.62, 128.01, 128.66, 128.75, 128.86, 130.82, 131.03, 136.68, 136.86, 136.97, 137.61, 154.27, 154.77. Two rotamers in a 56:44 ratio.

3-(((2-Cycloheptylethyl)(methyl)amino)methyl)-1*H*-indol-7-yl diethylcarbamate (11)
1*H*-Indol-7-ol (128 mg, 0.961 mmol), *N*,*N*-diethylcarbamoyl chloride (1.1 eq., 143 mg), and caesium carbonate (1.0 eq., 313 mg) in THF (3 mL) were stirred at rt under Ar for 18 h. 1*H*-Indol-7-yl diethylcarbamate was isolated by column chromatography on silica (1. PE/EtOAc = 10:1; 2. PE/EtOAc = 3:1). Yield: 48 mg (0.207 mmol, 21.5%) of beige semisolid that was immediately used further following *GP1* to prepare 3-(((2-cycloheptylethyl)(methyl)amino)methyl)-1*H*-indol-7-yl diethylcarbamate. Yield: 53 mg (0.133 mmol, 66.0%) of beige semisolid. ESI-HRMS: m/z = 400.2949 (MH$^+$); $C_{24}H_{38}N_3O_2$ requires: m/z = 400.2959 (MH$^+$). v_{max} 3323, 2973, 2919, 2851, 2787, 1700, 1474, 1457, 1417, 1348, 1273, 1218, 1156, 1096, 982, 757, 730 cm^{-1}. Purity: UPLC (220 nm): t_r = 4.753 min, 96.5% total area. ^{1}H NMR (400 MHz, CDCl$_3$) δ = 1.14 – 1.73 (m, 21H), 2.21 (s, 3H), 2.40 – 2.45 (m, 2H), 3.43 (q, *J*=7.0, 2H), 3.51 (q, *J*=6.9, 2H), 3.68 (s, 2H), 6.95 (dd, *J*=0.7, 7.7, 1H), 7.04 – 7.09 (m, 2H), 7.55 (d, *J*=7.9, 1H), 8.44 (s, 1H). ^{13}C NMR (101 MHz, CDCl$_3$) δ = 13.51, 14.45, 26.56, 28.60, 34.90, 35.86, 37.72, 42.28, 42.36, 42.53, 52.87, 55.82, 113.72, 114.01, 116.72, 119.51, 124.15, 129.01, 131.17, 137.13, 153.89.

3-(((2-Cycloheptylethyl)(methyl)amino)methyl)-1*H*-indol-7-yl diisopropylcarbamate (12)
1*H*-Indol-7-ol (95 mg, 0.713 mmol), *N*,*N*-diisopropylcarbamoyl chloride (1.5 eq., 175 mg), and DIPEA (500 µL) in MeCN (3 mL) were stirred at rt under Ar for 18 h. 1*H*-Indol-7-yl diisopropylcarbamate was isolated by column chromatography on silica (PE/EtOAc = 4:1). Yield: 51 mg (0.196 mmol, 27.5%) of beige solid. mp 92.8–95.1 °C. ESI-HRMS: m/z = 261.1594 (MH$^+$); $C_{15}H_{21}N_2O_2$ requires: m/z = 261.1598 (MH$^+$). v_{max} 3514, 3459, 3177, 2976, 2964, 2933, 1655, 1433, 1310, 1221, 1204, 1149, 1122, 1055, 1041, 897, 774, 717 cm^{-1}. ^{1}H NMR (400 MHz, CDCl$_3$) δ = 1.35 (br s, 6H), 1.41 (br s, 6H), 4.03 (br s, 1H), 4.19 (br s, 1H), 6.58 (dd, *J*=2.1, 3.2, 1H), 6.97 (dd, *J*=0.7, 7.7, 1H), 7.08 (t, *J*=7.8, 1H), 7.19 – 7.21 (m, 1H), 7.48 – 7.50 (m, 1H), 8.46 (s, 1H). ^{13}C NMR (101 MHz, CDCl$_3$) δ = 20.59, 21.84, 46.37, 47.30, 103.27, 113.73, 117.81, 119.90, 124.81, 128.80, 131.04, 137.17, 153.53.

3-(((2-Cycloheptylethyl)(methyl)amino)methyl)-1*H*-indol-7-yl diisopropylcarbamate was prepared following *GP1* from 1*H*-indol-7-yl diisopropylcarbamate (31 mg, 0.119 mmol). Yield:

13 mg (0.0304 mmol, 25.5%) of light brownish oil. ESI-HRMS: m/z = 428.3267 (MH$^+$); $C_{26}H_{42}N_3O_2$ requires: m/z = 428.3272 (MH$^+$). ν_{max} 3367, 2969, 2919, 2851, 2784, 1696, 1434, 1295, 1223, 1208, 1151, 1042, 1009, 823, 757, 730 cm^{-1}. Purity: UPLC (220 nm): t$_r$ = 4.937 min, 98.7% total area. ^{1}H NMR (400 MHz, CDCl$_3$) δ = 1.10 – 1.73 (m, 27H), 2.21 (s, 3H), 2.40 – 2.44 (m, 2H), 3.68 (s, 2H), 4.01 (br s, 1H), 4.17 (br s, 1H), 6.94 (dd, J=0.6, 7.5, 1H), 7.06 (t, J=7.8, 1H), 7.11 (d, J=2.2, 1H), 7.54 (d, J=7.9, 1H), 8.31 (s, 1H). ^{13}C NMR (101 MHz, CDCl$_3$) δ = 20.60, 21.84, 26.60, 28.63, 34.94, 35.91, 37.76, 42.41, 46.34, 47.29, 52.92, 55.84, 113.78, 114.14, 116.69, 119.60, 124.12, 129.20, 131.20, 137.05, 153.56.

3-(((2-Cycloheptylethyl)(methyl)amino)methyl)-1*H*-indol-7-yl piperidine-1-carboxylate (13)

1*H*-Indol-7-ol (117 mg, 0.879 mmol), piperidine-1-carbonyl chloride (1.1 eq., 143 mg), and caesium carbonate (1.0 eq., 286 mg) in THF (3 mL) were stirred at rt under Ar for 18 h. 1*H*-Indol-7-yl piperidine-1-carboxylate was isolated by column chromatography on silica (1. PE/EtOAc = 10:1; 2. PE/EtOAc = 3:1, yield: 174 mg, 0.712 mmol, 81.0%), and immediately used further following *GP1* to prepare 3-(((2-cycloheptylethyl)(methyl)amino)methyl)-1*H*-indol-7-yl piperidine-1-carboxylate. Yield: 98 mg (0.238 mmol, 47.6%) of brownish semisolid. ESI-HRMS: m/z = 412.2948 (MH$^+$); $C_{25}H_{38}N_3O_2$ requires: m/z = 412.2959 (MH$^+$). ν_{max} 3324, 2920, 2852, 2791, 1700, 1421, 1348, 1218, 1141, 1021, 953, 728 cm^{-1}. Purity: UPLC (254 nm): t$_r$ = 4.667 min, 99.8% total area. ^{1}H NMR (400 MHz, CDCl$_3$) δ = 1.14 – 1.23 (m, 2H), 1.35 – 1.72 (m, 19H), 2.21 (s, 3H), 2.39 – 2.45 (m, 2H), 3.54 (br s, 2H), 3.64 – 3.72 (m, 4H), 6.94 (dd, J=0.7, 7.7, 1H), 7.04 – 7.09 (m, 2H), 7.54 (d, J=7.6, 1H), 8.51 (s, 1H). ^{13}C NMR (101 MHz, CDCl$_3$) δ = 24.32, 25.58, 26.01, 26.52, 28.56, 34.86, 35.79, 37.69, 42.30, 45.30, 45.82, 52.81, 55.79, 113.77, 113.83, 116.66, 119.46, 124.15, 129.00, 131.06, 137.07, 153.36.

3-(((2-Cycloheptylethyl)(methyl)amino)methyl)-1*H*-indol-7-yl morpholine-4-carboxylate (14)

1*H*-Indol-7-ol (100 mg, 0.751 mmol), morpholine-4-carbonyl chloride (1.5 eq., 169 mg), and DIPEA (500 µL) in MeCN (3 mL) were stirred at rt under Ar for 18 h. 1*H*-Indol-7-yl morpholine-4-carboxylate was isolated by column chromatography on silica (1. PE/EtOAc = 5:1; 2. PE/EtOAc = 2:1). Yield: 106 mg (0.430 mmol, 57.3%) of beige solid. mp 151.2–152.5 °C. ESI-HRMS: m/z = 247.1074 (MH$^+$); $C_{13}H_{15}N_2O_3$ requires: m/z = 247.1077 (MH$^+$). ν_{max} 3332, 3295, 2989, 2957, 2919, 2865, 1693, 1412, 1342, 1230, 1210, 1113, 1082, 978, 855, 779, 720 cm^{-1}. ^{1}H NMR (400 MHz, CDCl$_3$) δ = 3.59 – 3.65 (m, 2H), 3.73 – 3.79 (m, 6H), 6.58 (dd, J=2.0, 3.1, 1H), 6.96 (d, J=7.7, 1H), 7.08 (t, J=7.8, 1H), 7.17 (t, J=2.6, 1H), 7.51 (d, J=7.9, 1H), 8.46 (s, 1H). ^{13}C NMR (101 MHz, CDCl$_3$) δ = 44.37, 45.17, 66.59, 66.72, 103.31, 113.78, 118.26, 119.89, 124.85, 128.45, 131.08, 136.87, 153.36.

3-(((2-Cycloheptylethyl)(methyl)amino)methyl)-1*H*-indol-7-yl morpholine-4-carboxylate was prepared following *GP1* from 1*H*-indol-7-yl morpholine-4-carboxylate (69 mg, 0.280 mmol). Yield: 36 mg (0.087 mmol, 31.1%) of beige solid. mp 111.2–112.9 °C. ESI-HRMS: m/z = 414.2744 (MH$^+$); $C_{24}H_{36}N_3O_3$ requires: m/z = 414.2751 (MH$^+$). ν_{max} 3327, 2917, 2857, 2797, 2767, 1699, 1452, 1417, 1352, 1245, 1220, 1162, 1119, 1101, 854, 782, 754, 736, 624 cm^{-1}. Purity: UPLC (220 nm): t$_r$ = 4.113 min, 99.9% total area. ^{1}H NMR (400 MHz, CDCl$_3$) δ = 1.13 – 1.22 (m, 2H), 1.34 – 1.71 (m, 13H), 2.21 (s, 3H), 2.40 – 2.44 (m, 2H), 3.61 (br s, 2H), 3.67 (s, 2H), 3.73 – 3.80 (m, 6H), 6.93 (d, J=7.1, 1H), 7.07 (t, J=7.8, 1H), 7.09 (d, J=2.2, 1H), 7.57 (d, J=7.9, 1H), 8.34 (s, 1H). ^{13}C NMR (101 MHz, CDCl$_3$) δ = 26.58, 28.62, 34.92, 35.90, 37.71, 42.44, 44.37, 45.18, 52.96, 55.90, 66.62, 66.76, 113.84, 114.37, 117.16, 119.60, 124.11, 128.86, 131.23, 136.77, 153.38.

3-(((2-Cycloheptylethyl)(methyl)amino)methyl)-1*H*-indol-7-yl methyl(prop-2-yn-1-yl)carbamate (15)

N-Methylpropargylamine (150 µL, 1.78 mmol) and CDI (1.0 eq., 289 mg) in DCM (5 mL) were stirred at rt for 12 h. The reaction mixture was extracted with water (10 mL, discarded), dried with sodium sulphate, the solvent was removed *in vacuo*, the residue dissolved in MeCN (5 mL), iodomethane (1.2 eq., 166 µL) was added, and the mixture stirred under Ar at rt for 18 h. The solvent was removed *in vacuo*, the residue redissolved in MeCN (5 mL), 1*H*-indol-7-ol (97 mg, 0.73 mmol) and DIPEA (500 µL) were added, and the reaction mixture stirred at 60 °C for 4 h. The solvent was removed *in vacuo* and 1*H*-indol-7-yl methyl(prop-2-yn-1-yl)carbamate isolated by column chromatography on silica (PE/EtOAc = 4:1). Yield: 119 mg (0.521 mmol, 82.1%) of beige semisolid, that was immediately used further following *GP1* to afford 3-(((2-cycloheptylethyl)(methyl)amino)methyl)-1*H*-indol-7-yl methyl(prop-2-yn-1-yl)carbamate. Yield: 111 mg (0.281 mmol, 53.9%) of beige oil. ESI-HRMS: *m/z* = 396.2640 (MH$^+$); C$_{24}$H$_{34}$N$_3$O$_2$ requires: *m/z* = 396.2646 (MH$^+$). ν_{max} 3306, 2919, 2850, 2788, 1706, 1634, 1580, 1443, 1394, 1348, 1218, 1167, 1138, 1031, 787, 731, 657 cm^{-1}. Purity: UPLC (220 nm): t$_r$ = 4.527 min, 99.9% total area. ^{1}H NMR (400 MHz, CDCl$_3$) δ = 1.14 – 1.24 (m, 2H), 1.35 – 1.74 (m, 13H), 2.21 (s, 3H), 2.32 – 2.46 (m, 3H), 3.09 and 3.20 (2 x s, 3H), 3.68 (s, 2H), 4.23 and 4.26 (2 x s, 2H), 6.95 – 7.04 (m, 2H), 7.07 (t, *J*=7.6, 1H), 7.57 (d, *J*=7.8, 1H), 8.56 and 8.60 (2 x s, 1H). ^{13}C NMR (101 MHz, CDCl$_3$) δ = 26.49, 28.53, 33.94, 34.65, 34.82, 35.78, 37.61, 38.59, 39.02, 42.27, 52.82, 55.77, 72.65, 72.82, 78.30, 78.92, 113.74, 113.98, 117.00, 119.37, 124.07, 124.20, 128.70, 128.82, 130.95, 131.11, 136.59, 136.78, 153.77, 154.11. Two sets of conformers.

3-(((2-Cycloheptylethyl)(methyl)amino)methyl)-1*H*-indol-7-yl methyl(pent-4-yn-1-yl)carbamate (16)

N-Methylpent-4-yn-1-amine[90] (486 mg, 5.0 mmol) and CDI (1.0 eq., 811 mg) in DCM (5 mL) were stirred at rt for 12 h. The reaction mixture was extracted with water (10 mL, discarded), dried with sodium sulphate, the solvent was removed *in vacuo*, the residue dissolved in MeCN (5 mL), iodomethane (1.2 eq., 374 µL) was added, and the mixture stirred under Ar at rt for 18 h. The solvent was removed *in vacuo*, the residue redissolved in MeCN (5 mL), 1*H*-indol-7-ol (157 mg, 1.18 mmol) and DIPEA (500 µL) were added, and the reaction mixture stirred at 60 °C for 4 h. The solvent was removed *in vacuo* and 1*H*-indol-7-yl methyl(pent-4-yn-1-yl)carbamate isolated by column chromatography on silica (PE/EtOAc = 4:1). Yield: 254 mg (0.991 mmol, 84.0%) of beige oil. ESI-HRMS: *m/z* = 257.1280 (MH$^+$); C$_{15}$H$_{17}$N$_2$O$_2$ requires: *m/z* = 257.1285 (MH$^+$). ν_{max} 3292, 2936, 1698, 1398, 1341, 1232, 1186, 1127, 1053, 786, 723, 636 cm^{-1}. ^{1}H NMR (400 MHz, CDCl$_3$) δ = 1.90 (dp, *J*=6.9, 14.1, 2H), 2.09 and 2.11 (t, *J*=2.6, 1H), 2.30 – 2.39 (m, 2H), 3.05 and 3.15 (2 x s, 3H), 3.51 (t, *J*=7.0, 1H), 3.63 (t, *J*=6.9, 1H), 6.56 – 6.59 (m, 1H), 7.02 (t, *J*=7.9, 1H), 7.07 – 7.14 (m, 2H), 7.52 (d, *J*=7.8, 1H), 8.67 and 8.73 (2 x s, 1H). ^{13}C NMR (101 MHz, CDCl$_3$) δ = 15.87, 15.99, 26.13, 26.63, 34.92, 34.95, 48.31, 48.68, 69.00, 69.40, 83.70, 83.77, 102.89, 102.93, 113.63, 117.82, 119.66, 124.72, 124.76, 128.42, 128.48, 130.80, 130.84, 137.04, 154.27, 154.32. Two sets of conformer signals.

3-(((2-Cycloheptylethyl)(methyl)amino)methyl)-1*H*-indol-7-yl methyl(pent-4-yn-1-yl)carbamate was prepared following *GP1* from 1*H*-indol-7-yl methyl(pent-4-yn-1-yl)carbamate (99 mg, 0.387 mmol). Yield: 103 mg (0.243 mmol, 38.2%) of beige oil. ESI-HRMS: *m/z* = 424.2951 (MH$^+$); C$_{26}$H$_{38}$N$_3$O$_2$ requires: *m/z* = 424.2959 (MH$^+$). ν_{max} 3309, 2920, 2851, 2789, 1705, 1444, 1399, 1349, 1303, 1223, 1187, 1127, 731, 632 cm^{-1}. Purity: UPLC (220 nm): t$_r$ = 4.687 min, 98.0% total area. ^{1}H NMR (400 MHz, CDCl$_3$) δ = 1.14 – 1.24 (m, 2H), 1.36 – 1.72 (m, 13H), 1.89 (dp, *J*=6.9, 20.8, 2H), 2.03 and 2.07 (t, *J*=2.5, 1H), 2.21 (s, 3H), 2.30 (td, *J*=2.6, 6.9, 1H), 2.34 (td, *J*=2.6, 6.7, 1H), 2.40 – 2.45 (m, 2H), 3.04 and 3.15 (s, 3H), 3.50 (t, *J*=7.0, 1H), 3.63 (t, *J*=6.9, 1H), 3.67 (s, 2H), 6.96 (t, *J*=8.0, 1H), 7.04 – 7.09 (m, 2H), 7.55 (d, *J*=7.8, 1H), 8.54 and 8.59 (s, 1H). ^{13}C NMR (101 MHz, CDCl$_3$) δ = 15.95, 16.06, 26.21, 26.51, 26.74, 28.55, 34.84, 35.04, 35.83, 37.63, 42.32, 48.39, 48.76, 52.86, 55.79, 69.01,

69.42, 83.65, 83.73, 113.71, 113.93, 113.99, 116.78, 119.41, 124.00, 124.07, 128.85, 128.90, 131.01, 131.07, 136.95, 154.32, 154.36.

3-(((2-Cycloheptylethyl)(methyl)amino)methyl)-1*H*-indol-7-yl methyl(undec-10-yn-1-yl)carbamate (17)

N-Methylundec-10-ynamide was prepared following *GP1* from undec-10-ynoic acid[91] (2000 mg, 10.97 mmol) and methylamine (2 M in THF), the solvent was removed *in vacuo*, residue partitioned between DCM (20 mL) and 10% citric acid (10 mL), the organic phase extracted with 1 M sodium hydroxide (10 mL), dried with sodium sulphate, and the solvent was removed *in vacuo*. The crude amide was dissolved in anhydrous THF (10 mL), lithium aluminum hydride solution (9.1 mL, 2.0 eq., 2.4 M in THF) was added slowly with stirring under Ar. The reaction mixture was stirred at 50 °C for 12 h and then while being cooled on an icebath, cautiously quenched with brine. The resulting grey solids were suspended in Et$_2$O (50 mL), sonicated in an ultrasonic cleaning bath for 5 minutes, filtered, and washed with Et$_2$O (2 × 20 mL). The ethereal extracts were dried over sodium sulphate, filtered, and volatile components evaporated *in vacuo* to afford *N*-methylundec-10-yn-1-amine[92].

To the crude *N*-methylundec-10-yn-1-amine (1432 mg) in DCM (20 mL) was added CDI (1.2 eq., 1536 mg), stirred for 6 h at rt, the reaction mixture was then extracted with water (40 mL), the organic phase separated, dried with sodium sulphate, and the solvent removed *in vacuo* to afford *N*-methyl-*N*-(undec-10-yn-1-yl)-1*H*-imidazole-1-carboxamide. Yield: 1840 mg (6.68 mmol, 60.9% over three steps) of white waxy semisolid.

3-Methyl-1-(methyl(undec-10-yn-1-yl)carbamoyl)-1*H*-imidazol-3-ium iodide was prepared by stirring *N*-methyl-*N*-(undec-10-yn-1-yl)-1*H*-imidazole-1-carboxamide (1000 mg, 3.63 mmol) and methyl iodide (1.5 eq., 339 μL) in MeCN (5 mL) under Ar for 24 h. The solvent was removed *in vacuo*, the residue dissolved in MeCN (5 mL), 1*H*-indol-7-ol (293 mg, 2.2 mmol) and DIPEA (500 μL) were added, and the reaction mixture stirred at 60 °C for 6 h. The solvent was removed *in vacuo* and 1*H*-indol-7-yl methyl(undec-10-yn-1-yl)carbamate isolated by column chromatography on silica (PE/EtOAc = 5:1). Yield: 539 mg (1.583 mmol, 72.0%) of colourless oil, that was immediately used further.

3-(((2-Cycloheptylethyl)(methyl)amino)methyl)-1*H*-indol-7-yl methyl(undec-10-yn-1-yl)carbamate was prepared following *GP1* from 1*H*-indol-7-yl methyl(undec-10-yn-1-yl)carbamate (300 mg, 0.881 mmol). Yield: 256 mg (0.504 mmol, 57.2%) of beige semisolid. ESI-HRMS: m/z = 508.3892 (MH$^+$); C$_{32}$H$_{50}$N$_3$O$_2$ requires: m/z = 508.3898 (MH$^+$). v_{max} 3309, 2922, 2853, 2786, 1705, 1460, 1400, 1350, 1306, 1223, 1169, 1123, 1093, 786, 756, 731, 628 cm^{-1}. Purity: UPLC (220 nm): t_r = 5.347 min, 99.7% total area. ^{1}H NMR (400 MHz, CDCl$_3$) δ = 1.14 – 1.72 (m, 29H), 1.96 (t, *J*=2.4, 1H), 2.15 – 2.23 (m, 5H), 2.41 – 2.45 (m, 2H), 3.01 and 3.10 (2 x s, 3H), 3.36 (t, *J*=7.4, 1H), 3.46 (t, *J*=7.2, 1H), 3.67 (s, 2H), 6.90 – 6.97 (m, 1H), 7.01 (d, *J*=1.9, 1H), 7.06 (t, *J*=7.8, 1H), 7.55 (dd, *J*=3.2, 7.8, 1H), 8.62 and 8.68 (2 x s, 1H). ^{13}C NMR (101 MHz, CDCl$_3$) δ = 18.32, 26.41, 26.62, 26.66, 27.33, 28.04, 28.37, 28.39, 28.45, 28.62, 28.96, 29.24, 29.37, 34.56, 34.60, 34.75, 34.84, 35.69, 37.54, 42.15, 49.46, 52.74, 55.65, 68.18, 84.60, 113.57, 113.65, 116.50, 116.62, 119.26, 124.12, 128.79, 128.90, 130.99, 136.97, 154.17, 154.32. Two conformers in a 53:47 ratio.

3-(((2-Cycloheptylethyl)(methyl)amino)methyl)-1*H*-indol-7-yl ethyl(prop-2-yn-1-yl)carbamate (18)

N-Ethylprop-2-yn-1-amine[93] (208 mg, 2.50 mmol) and CDI (1.0 eq., 405 mg) in DCM (5 mL) were stirred at rt for 12 h. The reaction mixture was extracted with water (10 mL, discarded), dried with sodium sulphate, the solvent was removed *in vacuo*, the residue dissolved in MeCN (5 mL), iodomethane (1.2 eq., 187 μL) was added, and the mixture stirred under Ar at rt for 18

h. The solvent was removed *in vacuo*, the residue redissolved in MeCN (5 mL), 1*H*-indol-7-ol (141 mg, 1.06 mmol) and DIPEA (500 µL) were added, and the reaction mixture stirred at 60 °C for 4 h. The solvent was removed *in vacuo* and 1*H*-indol-7-yl ethyl(prop-2-yn-1-yl)carbamate isolated by column chromatography on silica (PE/EtOAc = 4:1). Yield: 108 mg (0.446 mmol, 42.1%) of brownish oil, which was immediately used further in the next step.

3-(((2-Cycloheptylethyl)(methyl)amino)methyl)-1*H*-indol-7-yl ethyl(prop-2-yn-1-yl)carbamate was prepared following *GP1* from 1*H*-indol-7-yl ethyl(prop-2-yn-1-yl)carbamate (73 mg, 0.301 mmol). Yield: 64 mg (0.156 mmol, 51.9%) of beige oil. ESI-HRMS: *m/z* = 410.2797 (MH$^+$); C$_{25}$H$_{36}$N$_3$O$_2$ requires: *m/z* = 410.2802 (MH$^+$). v_{max} 3293, 2921, 2851, 2796, 2356, 2339, 1712, 1457, 1413, 1348, 1223, 1170, 1138 cm^{-1}.
Purity: UPLC (220 nm): t$_r$ = 4.667 min, 97.1% total area. ^{1}H NMR (400 MHz, CDCl$_3$) δ = 1.12 – 1.71 (m, 18H), 2.22 (s, 3H), 2.30 and 2.39 (2 × br s, 1H), 2.41 – 2.46 (m, 2H), 3.52 – 3.61 (m, 1H), 3.64 – 3.69 (m, 1H), 3.70 (s, 2H), 4.24 – 4.31 (m, 2H), 6.93 – 7.14 (m, 3H), 7.55 (d, *J*=7.8, 1H), 8.30 and 8.40 (2 × s, 1H). ^{13}C NMR (101 MHz, CDCl$_3$) δ = 26.55, 28.59, 34.88, 35.87, 36.53, 36.83, 37.67, 42.14, 42.37, 42.79, 42.97, 52.90, 55.82, 72.01, 72.42, 78.95, 80.03, 113.71, 113.91, 114.09, 114.14, 116.54, 116.81, 117.03, 119.48, 123.97, 128.89, 128.94, 130.95, 131.18, 133.52, 134.25, 136.67, 136.87, 153.29, 153.90. A mixture of conformers.

3-(((2-Cycloheptylethyl)(methyl)amino)methyl)-1*H*-indol-7-yl di(prop-2-yn-1-yl)carbamate (19)

Di(prop-2-yn-1-yl)amine (372 mg, 4.0 mmol) and CDI (1.0 eq., 649 mg) in DCM (5 mL) were stirred at rt for 12 h. The reaction mixture was extracted with water (10 mL, discarded), dried with sodium sulphate, the solvent was removed *in vacuo*, the residue dissolved in MeCN (5 mL), iodomethane (1.2 eq., 299 µL) was added, and the mixture stirred under Ar at rt for 18 h. The solvent was removed *in vacuo*, the residue redissolved in MeCN (5 mL), 1*H*-indol-7-ol (293 mg, 2.2 mmol) and DIPEA (500 µL) were added, and the reaction mixture stirred at 60 °C for 4h. The solvent was removed *in vacuo* and 1*H*-indol-7-yl di(prop-2-yn-1-yl)carbamate isolated by column chromatography on silica (PE/EtOAc = 4:1). Yield: 363 mg (1.44 mmol, 65.4%) of beige solid. mp 78.1–79.5 °C. ESI-HRMS: *m/z* = 253.0958 (MH$^+$); C$_{15}$H$_{13}$N$_2$O$_2$ requires: *m/z* = 253.0972 (MH$^+$). v_{max} 3303, 3286, 2975, 1691, 1458, 1407, 1340, 1211, 1159, 1103, 963, 850, 788, 723, 638 cm^{-1}. ^{1}H NMR (400 MHz, CDCl$_3$) δ = 2.42 and 2.46 (2 x s, 2H), 4.41 and 4.46 (2 x s, 4H), 6.59 (dd, *J*=2.1, 3.1, 1H), 7.07 – 7.16 (m, 3H), 7.56 (d, *J*=7.6, 1H), 8.57 (s, 1H). ^{13}C NMR (101 MHz, CDCl$_3$) δ = 36.10, 36.29, 72.87, 73.40, 77.84, 78.68, 103.03, 113.93, 118.34, 119.70, 124.86, 128.20, 130.80, 136.47, 153.20.

3-(((2-Cycloheptylethyl)(methyl)amino)methyl)-1*H*-indol-7-yl di(prop-2-yn-1-yl)carbamate was prepared following *GP1* from 1*H*-indol-7-yl di(prop-2-yn-1-yl)carbamate (150 mg, 0.595 mmol). Yield: 165 mg (0.393 mmol, 66.1%) of beige oil. ESI-HRMS: *m/z* = 420.2625 (MH$^+$); C$_{26}$H$_{34}$N$_3$O$_2$ requires: *m/z* = 420.2646 (MH$^+$). v_{max} 3303, 2920, 2851, 2794, 1716, 1443, 1407, 1345, 1216, 1168, 1101, 731 cm^{-1}. Purity: UPLC (220 nm): t$_r$ = 4.593 min, 98.5% total area. ^{1}H NMR (400 MHz, CDCl$_3$) δ = 1.16 – 1.24 (m, 2H), 1.37 – 1.74 (m, 13H), 2.21 (s, 3H), 2.35 – 2.47 (m, 4H), 3.68 (s, 2H), 4.37 and 4.43 (2 x s, 4H), 7.00 – 7.05 (m, 2H), 7.09 (t, *J*=7.8, 1H), 7.59 (d, *J*=7.7, 1H), 8.58 (s, 1H). ^{13}C NMR (101 MHz, CDCl$_3$) δ = 26.47, 28.50, 34.80, 35.75, 36.06, 36.23, 37.57, 42.23, 52.79, 55.74, 72.83, 73.34, 77.82, 78.65, 113.95, 113.99, 117.24, 119.36, 124.10, 128.62, 130.97, 136.38, 153.20.

3-(((2-Cycloheptylethyl)(methyl)amino)methyl)-1*H*-indol-7-yl isopropyl(prop-2-yn-1-yl)carbamate (20)

N-Isopropylprop-2-yn-1-amine[94] (768 mg, 7.90 mmol) and CDI (1.0 eq., 1281 mg) in DCM (8 mL) were stirred at rt for 12 h. The reaction mixture was extracted with water (15 mL,

discarded), dried with sodium sulphate, the solvent was removed *in vacuo*, the residue dissolved in MeCN (5 mL), iodomethane (1.2 eq., 590 µL) was added, and the mixture stirred under Ar at rt for 18 h. The solvent was removed *in vacuo*, the residue redissolved in MeCN (5 mL), 1*H*-indol-7-ol (181 mg, 1.36 mmol) and DIPEA (500 µL) were added, and the reaction mixture stirred at 60 °C for 4 h. The solvent was removed *in vacuo* and 1*H*-indol-7-yl isopropyl(prop-2-yn-1-yl)carbamate isolated by column chromatography on silica (PE/EtOAc = 3:1). Yield: 290 mg (1.13 mmol, 83.1%) of brownish oil. ESI-HRMS: m/z = 257.1281 (MH$^+$); $C_{15}H_{17}N_2O_2$ requires: m/z = 257.1285 (MH$^+$). v_{max} 3421, 3297, 2979, 1698, 1441, 1404, 1332, 1233, 1193, 1067, 891, 781, 722 cm^{-1}. Purity: UPLC (254 nm): t_r = 4.493 min, 99.5% total area. ^{1}H NMR (400 MHz, CDCl$_3$) δ = 1.29 – 1.47 (m, 6H), 2.35 and 2.43 (br s, 1H), 4.15 (s, 2H), 4.54 (hept, *J*=6.6, 1H), 6.59 – 6.63 (m, 1H), 7.03 – 7.21 (m, 3H), 7.54 – 7.58 (m, 1H), 8.62 and 8.74 (s, 1H). ^{13}C NMR (101 MHz, CDCl$_3$) δ = 20.18, 20.86, 31.78, 32.58, 48.34, 49.09, 71.05, 80.58, 81.86, 102.89, 113.55, 114.00, 117.82, 119.60, 124.58, 124.87, 128.48, 130.52, 130.88, 136.73, 153.12, 153.72. Two sets of conformer signals.

3-(((2-Cycloheptylethyl)(methyl)amino)methyl)-1*H*-indol-7-yl isopropyl(prop-2-yn-1-yl)carbamate was prepared following *GP1* from 1*H*-indol-7-yl isopropyl(prop-2-yn-1-yl)carbamate (141 mg, 0.550 mmol). Yield: 120 mg (0.283 mmol, 51.5%) of beige semisolid. ESI-HRMS: m/z = 424.29504 (MH$^+$); $C_{26}H_{38}N_3O_2$ requires: m/z = 424.2959 (MH$^+$). v_{max} 3308, 2919, 2851, 2788, 1705, 1443, 1406, 1334, 1225, 1197, 1168, 11083, 756, 732 cm^{-1}. Purity: UPLC (220 nm): t_r = 4.723 min, 98.0% total area. ^{1}H NMR (400 MHz, CDCl$_3$) δ = 1.14 – 1.73 (m, 21H), 2.22 (s, 3H), 2.38 and 2.51 (2 x s, 1H), 2.40 – 2.45 (m, 2H), 3.68 (s, 2H), 4.14 (d, *J*=2.4, 2H), 4.50 (hept, *J*=6.8, 1H), 6.94 – 7.11 (m, 3H), 7.57 (d, *J*=8.6, 1H), 8.47 and 8.55 (s, 1H). ^{13}C NMR (101 MHz, CDCl$_3$) δ = 20.37, 21.02, 26.52, 31.96, 32.70, 34.86, 35.86, 37.65, 42.33, 48.44, 49.20, 52.88, 55.78, 71.07, 82.01, 114.08, 114.14, 116.88, 119.44, 123.83, 128.95, 130.81, 136.71, 153.20.

3-(((2-Cycloheptylethyl)(methyl)amino)methyl)-1*H*-indol-7-yl methoxy(methyl)carbamate (21)

1-(Methoxy(methyl)carbamoyl)-3-methyl-1*H*-imidazol-3-ium iodide[58] (3.0 eq., 713 mg), 1*H*-indol-7-ol (106 mg, 0.8 mmol), and DIPEA (500 µL) in MeCN (5 mL) were stirred at 60 °C for 4 h. The solvent was removed *in vacuo* and 1*H*-indol-7-yl methoxy(methyl)carbamate isolated by column chromatography on silica (1. PE/EtOAc = 3:1; 2. PE/EtOAc = 1:1). Yield: 156 mg (0.708 mmol, 88.5%) of beige semisolid. ESI-HRMS: m/z = 221.0916 (MH$^+$); $C_{11}H_{13}N_2O_3$ requires: m/z = 221.0921 (MH$^+$). v_{max} 3308, 2940, 1705, 1580, 1458, 1418, 1369, 1341, 1234, 1215, 1164, 1140, 1110, 1042, 1015, 939, 784, 732 cm^{-1}. ^{1}H NMR (400 MHz, CDCl$_3$) δ = 3.32 (s, 3H), 3.81 (s, 3H), 6.56 (dd, *J*=2.1, 3.1, 1H), 7.04 – 7.14 (m, 3H), 7.53 – 7.56 (m, 1H), 8.85 (s, 1H). ^{13}C NMR (101 MHz, CDCl$_3$) δ = 35.60, 61.69, 102.79, 113.62, 118.25, 119.55, 125.05, 128.21, 130.93, 136.45, 154.71.

3-(((2-Cycloheptylethyl)(methyl)amino)methyl)-1*H*-indol-7-yl methoxy(methyl)carbamate was prepared following *GP1* from 1*H*-indol-7-yl methoxy(methyl)carbamate (108 mg, 0.490 mmol). Yield: 120 mg (0.310 mmol, 63.3%) of yellowish oil. ESI-HRMS: m/z = 388.2583 (MH$^+$); $C_{22}H_{34}N_3O_3$ requires: m/z = 388.2595 (MH$^+$). v_{max} 3327, 2919, 2851, 2790, 1724, 1579, 1445, 1346, 1224, 1169, 1045, 980, 731 cm^{-1}. Purity: UPLC (220 nm): t_r = 4.443 min, 99.5% total area. ^{1}H NMR (400 MHz, CDCl$_3$) δ = 1.14 – 1.24 (m, 2H), 1.35 – 1.73 (m, 13H), 2.21 (s, 3H), 2.40 – 2.45 (m, 2H), 3.30 (s, 3H), 3.67 (s, 2H), 3.81 (s, 3H), 7.00 (dd, *J*=0.6, 7.7, 1H), 7.04 (d, *J*=2.1, 1H), 7.08 (t, *J*=7.8, 1H), 7.58 (d, *J*=7.7, 1H), 8.76 (s, 1H). ^{13}C NMR (101 MHz, CDCl$_3$) δ = 26.49, 28.52, 34.82, 35.74, 37.63, 42.24, 52.74, 55.77, 61.84, 113.72, 113.80, 117.16, 119.34, 124.34, 128.61, 131.13, 136.40, 154.80.

3-(((2-Cycloheptylethyl)(methyl)amino)methyl)-1*H*-indol-7-yl 1,2,2-trimethylhydrazine-1-carboxylate (22)

1,1,2-Trimethylhydrazine[95] (3.76 mmol) and CDI (1.0 eq., 610 mg) in DCM (10 mL) were stirred at rt for 12 h. The reaction mixture was extracted with water (10 mL, discarded), dried with sodium sulphate, the solvent was removed *in vacuo*, the residue dissolved in MeCN (5 mL), iodomethane (1.1 eq., 257 µL) was added, and the mixture stirred under Ar at rt for 12 h. Then 1*H*-indol-7-ol (200 mg, 1.5 mmol) and DIPEA (500 µL) were added, and the reaction mixture stirred at 60 °C for 4 h. The solvent was removed *in vacuo* and 1*H*-indol-7-yl 1,2,2-trimethylhydrazine-1-carboxylate isolated by column chromatography on silica (1. PE/EtOAc = 3:1; 2. PE/EtOAc = 1:1). Yield: 211 mg (0.905 mmol, 60.3%) of brownish semisolid. ^{1}H NMR (400 MHz, CDCl$_3$) δ = 2.66 (s, 6H), 3.02 and 3.13 (2 x br s, 3H), 6.52 (dd, *J*=2.1, 3.1, 1H), 6.98 (d, *J*=7.6, 1H), 7.05 (t, *J*=7.7, 1H), 7.11 (t, *J*=2.8, 1H), 7.47 (d, *J*=7.8, 1H), 8.98 (s, 1H).

3-(((2-Cycloheptylethyl)(methyl)amino)methyl)-1*H*-indol-7-yl 1,2,2-trimethylhydrazine-1-carboxylate was prepared following *GP1* from 1*H*-indol-7-yl 1,2,2-trimethylhydrazine-1-carboxylate (211 mg, 0.905 mmol). Yield: 184 mg (0.459 mmol, 50.8%) of brownish semisolid. ESI-HRMS: *m/z* = 401.2902 (MH$^+$); C$_{23}$H$_{37}$N$_4$O$_2$ requires: *m/z* = 401.2911 (MH$^+$). v_{max} 3170, 2920, 2851, 2783, 1718, 1579, 1445, 1347, 1227, 1121, 1021, 908, 730 cm^{-1}. Purity: UPLC (220 nm): t$_r$ = 4.420 min, 99.0% total area. ^{1}H NMR (400 MHz, CDCl$_3$) δ = 1.11 – 1.22 (m, 2H), 1.34 – 1.72 (m, 13H), 2.18 (s, 3H), 2.38 – 2.43 (m, 2H), 2.66 (s, 6H), 2.96 – 3.25 (m, 3H), 3.65 (s, 2H), 6.96 (d, *J*=7.1, 1H), 7.02 – 7.07 (m, 2H), 7.52 (dd, *J*=0.8, 7.8, 1H), 8.82 (s, 1H). ^{13}C NMR (101 MHz, CDCl$_3$) δ = 26.41, 27.82, 28.45, 31.91, 34.73, 35.62, 37.58, 42.14, 42.44, 43.02, 52.63, 55.67, 113.48, 113.73, 116.63, 119.22, 124.26, 128.79, 130.98, 136.81, 154.72.

3-(((2-Cycloheptylethyl)(methyl)amino)methyl)-1*H*-indol-6-yl dimethylcarbamate (23)

1*H*-Indol-6-ol (prepared from 6-benzyloxyindole as described under **6**, 149 mg, 1.12 mmol), *N,N*-dimethylcarbamoyl chloride (1.1 eq., 103 µL), and DIPEA (500 µL) in MeCN (3 mL) were stirred at rt under Ar for 18 h. 1*H*-Indol-6-yl dimethylcarbamate was isolated by column chromatography on silica (PE/EtOAc = 3:1). Yield: 196 mg (0.960 mmol, 85.7%) of beige semisolid, which was immediately used further following *GP1* to afford 3-(((2-cycloheptylethyl)(methyl)amino)methyl)-1*H*-indol-6-yl dimethylcarbamate. Yield: 199 mg (0.536 mmol, 55.8%) of beige semisolid. ESI-HRMS: *m/z* = 372.2636 (MH$^+$); C$_{22}$H$_{34}$N$_3$O$_2$ requires: *m/z* = 372.2646 (MH$^+$). v_{max} 3310, 2918, 2851, 2788, 1697, 1626, 1456, 1393, 1343, 1186, 945, 874, 840 cm^{-1}. Purity: UPLC (220 nm): t$_r$ = 4.403 min, 95.7% total area. ^{1}H NMR (400 MHz, CDCl$_3$) δ = 1.14 – 1.23 (m, 2H), 1.35 – 1.74 (m, 12H), 2.18 (s, 3H), 2.40 – 2.45 (m, 2H), 3.04 (s, 3H), 3.12 (s, 3H), 3.62 (s, 2H), 6.80 (d, *J*=1.4, 1H), 6.83 (dd, *J*=2.1, 8.5, 2H), 6.98 (d, *J*=2.0, 1H), 7.57 (d, *J*=8.5, 1H), 9.28 (s, 1H). ^{13}C NMR (101 MHz, CDCl$_3$) δ = 26.45, 28.50, 34.79, 35.65, 36.46, 36.72, 37.68, 42.06, 52.50, 55.72, 104.59, 111.95, 113.55, 119.24, 124.75, 125.76, 136.12, 146.81, 156.05.

3-(((2-Cycloheptylethyl)(methyl)amino)methyl)-1*H*-indol-6-yl diisopropylcarbamate (24)

1*H*-Indol-6-ol (122 mg, 0.916 mmol), *N,N*-diisopropylcarbamoyl chloride (1.5 eq., 225 mg), and DIPEA (500 µL) in MeCN (3 mL) were stirred at rt under Ar for 18 h. 1*H*-Indol-6-yl diisopropylcarbamate was isolated by column chromatography on silica (PE/EtOAc = 4:1). Yield: 70 mg (0.269 mmol, 29.4%) of white solid. ESI-HRMS: *m/z* = 261.1594 (MH$^+$); C$_{15}$H$_{21}$N$_2$O$_2$ requires: *m/z* = 261.1598 (MH$^+$). v_{max} 3365, 2992, 2971, 1696, 1457, 1284, 1137, 1087, 1020, 894, 866, 782, 722 cm^{-1}. Purity: UPLC (220 nm): t$_r$ = 4.703 min, 99.3% total area. ^{1}H NMR (400 MHz, DMSO) δ = 1.20 – 1.33 (m, 12H), 3.96 – 4.05 (m, 2H), 6.41 (ddd, *J*=0.9, 1.9, 3.0, 1H), 6.71 (dd, *J*=2.1, 8.5, 1H), 7.07 – 7.09 (m, 1H), 7.32 – 7.34 (m, 1H), 7.47 (d, *J*=8.5,

1H), 11.03 (s, 1H). ^{13}C NMR (101 MHz, DMSO) δ = 20.21, 21.18, 45.89, 100.96, 104.34, 113.75, 119.89, 124.94, 125.69, 135.69, 146.23, 153.56.

3-(((2-Cycloheptylethyl)(methyl)amino)methyl)-1H-indol-6-yl diisopropylcarbamate was prepared following *GP1* from 1H-indol-6-yl diisopropylcarbamate (50 mg, 0.192 mmol). Yield: 59 mg (0.138 mmol, 71.9%) of beige semisolid. ESI-HRMS: *m/z* = 428.3265 (MH$^+$); $C_{26}H_{42}N_3O_2$ requires: *m/z* = 428.3272 (MH$^+$). v_{max} 3290, 2969, 2920, 2852, 2761, 1684, 1431, 1369, 1331, 1301, 1228, 1210, 1146, 1042, 994, 868, 784, 760, 729 cm^{-1}. Purity: UPLC (254 nm): t_r = 4.870 min, 100.0% total area. ^{1}H NMR (400 MHz, CDCl$_3$) δ = 1.13 – 1.72 (m, 27H), 2.18 (s, 3H), 2.38 – 2.44 (m, 2H), 3.63 (s, 2H), 3.98 (br s, 1H), 4.17 (br s, 1H), 6.85 (dd, *J*=2.1, 8.5, 1H), 6.89 (d, *J*=2.2, 1H), 7.06 (d, *J*=1.9, 1H), 7.60 (d, *J*=8.5, 1H), 8.77 (s, 1H). ^{13}C NMR (101 MHz, CDCl$_3$) δ = 20.64, 21.62, 26.56, 28.62, 34.90, 35.87, 37.71, 42.25, 45.99, 46.96, 52.79, 55.83, 104.60, 112.75, 113.92, 119.57, 124.34, 125.75, 136.31, 146.96, 154.97.

3-(((2-Cycloheptylethyl)(methyl)amino)methyl)-1H-indol-6-yl methyl(prop-2-yn-1-yl)carbamate (25)

N-Methylpropargylamine (200 µL, 2.37 mmol) and CDI (1.0 eq., 384 mg) in DCM (5 mL) were stirred at rt for 12 h. The reaction mixture was extracted with water (10 mL, discarded), dried with sodium sulphate, the solvent was removed *in vacuo*, the residue dissolved in MeCN (5 mL), iodomethane (1.5 eq., 221 µL) was added, and the mixture stirred under Ar at rt for 18 h. The solvent was removed *in vacuo*, the residue redissolved in MeCN (5 mL), 1H-indol-6-ol (146 mg, 1.1 mmol) and DIPEA (500 µL) were added, and the reaction mixture stirred at 60 °C for 4 h. The solvent was removed *in vacuo* and 1H-indol-6-yl methyl(prop-2-yn-1-yl)carbamate isolated by column chromatography on silica (PE/EtOAc = 3:1). Yield: 200 mg (0.876 mmol, 79.7%) of white solid. mp 145.5–146.1 °C. ESI-HRMS: *m/z* = 229.0968 (MH$^+$); $C_{13}H_{13}N_2O_2$ requires: *m/z* = 229.0972 (MH$^+$). v_{max} 3360, 3293, 3076, 1698, 1453, 1394, 1342, 1286, 1237, 1215, 1152, 1089, 797, 725, 651 cm^{-1}. Purity: UPLC (254 nm): t_r = 4.030 min, 96.9% total area. ^{1}H NMR (400 MHz, CDCl$_3$) δ = 2.34 and 2.36 (2 x s, 1H), 3.12 and 3.22 (2 x s, 3H), 4.26 and 4.30 (2 x s, 2H), 6.40 – 6.43 (m, 1H), 6.85 (d, *J*=8.5, 1H), 6.97 – 6.99 (m, 1H), 7.07 (s, 1H), 7.53 (d, *J*=8.5, 1H), 8.54 (s, 1H).

3-(((2-Cycloheptylethyl)(methyl)amino)methyl)-1H-indol-6-yl methyl(prop-2-yn-1-yl)carbamate was prepared following *GP1* from 1H-indol-6-yl methyl(prop-2-yn-1-yl)carbamate (109 mg, 0.47 mmol). Yield: 20 mg (0.0506 mmol, 10.8%) of beige semisolid. ESI-HRMS: *m/z* = 396.2637 (MH$^+$); $C_{24}H_{34}N_3O_2$ requires: *m/z* = 396.2646 (MH$^+$). v_{max} 3249, 2919, 2850, 2789, 1702, 1456, 1419, 1399, 1343, 1236, 1167, 1125, 1027, 874, 798, 756, 731 cm^{-1}. Purity: UPLC (254 nm): t_r = 4.447 min, 99.6% total area. ^{1}H NMR (400 MHz, CDCl$_3$) δ = 1.12 – 1.22 (m, 2H), 1.34 – 1.71 (m, 13H), 2.19 (s, 3H), 2.32 (br s, 1H), 2.39 – 2.44 (m, 2H), 3.10 and 3.20 (2 x s, 3H), 3.64 (s, 2H), 4.25 and 4.29 (2 x s, 2H), 6.85 (dd, *J*=1.8, 8.6, 1H), 6.98 (d, *J*=2.2, 1H), 7.06 (d, *J*=1.8, 1H), 7.61 (d, *J*=8.6, 1H), 8.52 and 8.55 (s, 1H). ^{13}C NMR (101 MHz, CDCl$_3$) δ = 26.58, 28.63, 33.87, 34.35, 34.91, 35.85, 37.73, 38.59, 38.81, 42.33, 52.81, 55.89, 72.51, 72.62, 78.67, 104.46, 113.13, 113.88, 119.75, 124.37, 126.00, 136.18, 147.01, 155.12, 155.47. Two sets of conformer signals.

N-(9-(2-(4-(2-Azidoethyl)piperazine-1-carbonyl)phenyl)-6-(diethylamino)-3H-xanthen-3-ylidene)-*N*-ethylethanaminium chloride (26)

N-(9-(2-Carboxyphenyl)-6-(diethylamino)-3H-xanthen-3-ylidene)-*N*-ethylethanaminium chloride/rhodamine B (7000 mg, 14.6 mmol), oxalyl chloride (3.0 eq., 3.71 mL) and DMF (100 µL) in DCM (50 mL) were stirred under Ar at rt for 3 h (gas effervescence!), then the volatiles were removed *in vacuo*, the residue was dissolved in toluene (50 mL), the solvent removed *in vacuo*, the residue redissolved in DCM (50 mL), 1-(2-azidoethyl)piperazine[96] (1.2 eq., 2719 mg) and triethylamine (3.0 eq., 4.07 mL) were added, and the stirring continued at rt for 18 h. The solvent was removed *in vacuo* and the product isolated by column chromatography on

silica (1. EtOAc/Et$_3$N = 100:1; 2. DCM/MeOH = 20:1; 3. DCM/MeOH = 9:1) and *GP2*. Yield: 2657 mg (4.31 mmol, 29.5%) of dark violet semisolid. v_{max} 3415, 3081, 2977, 2931, 2102, 1689, 1627, 1584, 1528, 1508, 1466, 1411, 1335, 1273, 1247, 1178, 1121, 1072, 1010, 921, 820, 798, 682 cm^{-1}. ESI-HRMS: *m/z* = 580.3409 (M$^+$); C$_{34}$H$_{42}$N$_7$O$_2$ requires: *m/z* = 580.3395 (M$^+$). Purity: UPLC (220 nm): t$_r$ = 4.443 min, 96.8% total area. ^{1}H NMR (400 MHz, CDCl$_3$) δ = 1.31 (t, *J*=7.1, 12H), 2.34 (s, 4H), 2.51 – 2.55 (m, 2H), 3.28 – 3.32 (m, 2H), 3.32 – 3.35 (m, 2H), 3.40 – 3.44 (m, 2H), 3.61 (qd, *J*=2.5, 7.3, 8H), 6.78 (d, *J*=2.4, 2H), 6.93 (dd, *J*=2.3, 9.5, 2H), 7.22 (d, *J*=9.5, 2H), 7.32 – 7.34 (m, 1H), 7.51 – 7.54 (m, 1H), 7.63 – 7.68 (m, 2H). ^{13}C NMR (101 MHz, CDCl$_3$) δ = 12.71, 29.80, 41.82, 46.20, 47.63, 48.10, 53.04, 56.97, 96.46, 113.86, 114.17, 127.70, 130.03, 130.24, 130.36, 130.71, 132.25, 135.52, 155.76, 156.08, 157.87, 167.48.

Associated content

The Supporting Information is available free of charge … at DOI: XXXXX.

> Time-dependency experiments figures, additional figures from kinetic evaluation and mass spectrometry, trial fluorescent labelling of BChE – raw data, data collection and refinement statistics for X-ray structure determination, custom chemistry file for CovDock covalent docking, additional figures from MD simulations, DFT-calculated energies and coordinates of the optimised chemical species in the studied model reaction, representative NMR spectra and HPLC chromatograms (**PDF**).

> Molecular formula strings (**CSV**).

PDB ID codes: 8AI7. Authors will release the atomic coordinates and experimental data upon article publication.

Acknowledgement

Abbreviations Used

ACh – acetylcholine

(h)AChE – (human) acetylcholinesterase

(h)BChE – (human) butyrylcholinesterase

BW284c51 – 1,5-bis(4-allyldimethylammoniumphenyl)pentan-3-one dibromide

ChE(s) – cholinesterase(s)

ChEI(s) – cholinesterase inhibitor(s)

EtOAc – ethyl acetate

EtOH – ethanol

IRC – intrinsic reaction coordinate

isoOMPA – tetraisopropyl pyrophosphoramide

MES – 2-(N-morpholino)ethanesulfonic acid

MeCN – acetonitrile

MeOH – methanol

PE – petroleum ether

RA – residual activity

RMSD – root-mean-square deviation

SEM – standard error of the mean

References

(1) Xing, S.; Li, Q.; Xiong, B.; Chen, Y.; Feng, F.; Liu, W.; Sun, H. Structure and Therapeutic Uses of Butyrylcholinesterase: Application in Detoxification, Alzheimer's Disease, and Fat Metabolism. *Med. Res. Rev.* **2021**, *41* (2), 858–901. https://doi.org/10.1002/med.21745.

(2) Lockridge, O. Review of Human Butyrylcholinesterase Structure, Function, Genetic Variants, History of Use in the Clinic, and Potential Therapeutic Uses. *Pharmacol. Ther.* **2015**, *148*, 34–46. https://doi.org/10.1016/j.pharmthera.2014.11.011.

(3) Miles, J. A.; Ross, B. P. Recent Advances in Virtual Screening for Cholinesterase Inhibitors. *ACS Chem. Neurosci.* **2021**, *12* (1), 30–41. https://doi.org/10.1021/acschemneuro.0c00627.

(4) Jing, L.; Wu, G.; Kang, D.; Zhou, Z.; Song, Y.; Liu, X.; Zhan, P. Contemporary Medicinal-Chemistry Strategies for the Discovery of Selective Butyrylcholinesterase Inhibitors. *Drug Discov. Today* **2019**, *24* (2), 629–635. https://doi.org/10.1016/j.drudis.2018.11.012.

(5) Li, Q.; Xiong, B.; Wang, Y.; Lyu, W.; Xing, S.; Chen, Y.; Liao, Q.; He, S.; Feng, F.; Liu, W.; Chen, Y.; Sun, H. A Highly Effective and Stable Butyrylcholinesterase Inhibitor with Multi-Faceted Neuroprotection and Cognition Improvement. *Eur. J. Med. Chem.* **2022**, *239*, 114510. https://doi.org/10.1016/j.ejmech.2022.114510.

(6) Fernández-Bolaños, J. G.; López, Ó. Butyrylcholinesterase Inhibitors as Potential Anti-Alzheimer's Agents: An Updated Patent Review (2018-Present). *Expert Opin. Ther. Pat.* **2022**, *32* (8), 913–932. https://doi.org/10.1080/13543776.2022.2083956.

(7) Moreira, N. C. dos S.; Lima, J. E. B. de F.; Marchiori, M. F.; Carvalho, I.; Sakamoto-Hojo, E. T. Neuroprotective Effects of Cholinesterase Inhibitors: Current Scenario in Therapies for Alzheimer's Disease and Future Perspectives. *J. Alzheimers Dis. Rep.* **2022**, *6* (1), 177–193. https://doi.org/10.3233/ADR-210061.

(8) Sun, H.; Pang, Y.-P.; Lockridge, O.; Brimijoin, S. Re-Engineering Butyrylcholinesterase as a Cocaine Hydrolase. *Mol. Pharmacol.* **2002**, *62* (2), 220–224. https://doi.org/10.1124/mol.62.2.220.

(9) Zhang, T.; Zheng, X.; Kim, K.; Zheng, F.; Zhan, C.-G. Blocking Drug Activation as a Therapeutic Strategy to Attenuate Acute Toxicity and Physiological Effects of Heroin. *Sci. Rep.* **2018**, *8* (1), 16762. https://doi.org/10.1038/s41598-018-35196-8.

(10) Zhang, H.; Wang, Y.; Wang, Y.; Li, X.; Wang, S.; Wang, Z. Recent Advance on Carbamate-Based Cholinesterase Inhibitors as Potential Multifunctional Agents against Alzheimer's Disease. *Eur. J. Med. Chem.* **2022**, *240*, 114606. https://doi.org/10.1016/j.ejmech.2022.114606.

(11) Scheindlin, S. Episodes in the Story of Physostigmine. *Mol. Interv.* **2010**, *10* (1), 4. https://doi.org/10.1124/mi.10.1.1.

(12) Bar-On, P.; Millard, C. B.; Harel, M.; Dvir, H.; Enz, A.; Sussman, J. L.; Silman, I. Kinetic and Structural Studies on the Interaction of Cholinesterases with the Anti-Alzheimer Drug Rivastigmine,. *Biochemistry* **2002**, *41* (11), 3555–3564. https://doi.org/10.1021/bi020016x.

(13) Košak, U.; Strašek, N.; Knez, D.; Jukič, M.; Žakelj, S.; Zahirović, A.; Pišlar, A.; Brazzolotto, X.; Nachon, F.; Kos, J.; Gobec, S. N-Alkylpiperidine Carbamates as Potential Anti-Alzheimer's Agents. *Eur. J. Med. Chem.* **2020**, *197*, 112282. https://doi.org/10.1016/j.ejmech.2020.112282.

(14) Awoonor-Williams, E.; Walsh, A. G.; Rowley, C. N. Modeling Covalent-Modifier Drugs. *Biochim. Biophys. Acta BBA - Proteins Proteomics* **2017**, *1865* (11, Part B), 1664–1675. https://doi.org/10.1016/j.bbapap.2017.05.009.

(15) De Cesco, S.; Kurian, J.; Dufresne, C.; Mittermaier, A. K.; Moitessier, N. Covalent Inhibitors Design and Discovery. *Eur. J. Med. Chem.* **2017**, *138*, 96–114. https://doi.org/10.1016/j.ejmech.2017.06.019.

(16) Flanagan, M. E.; Abramite, J. A.; Anderson, D. P.; Aulabaugh, A.; Dahal, U. P.; Gilbert, A. M.; Li, C.; Montgomery, J.; Oppenheimer, S. R.; Ryder, T.; Schuff, B. P.; Uccello, D. P.; Walker, G. S.; Wu, Y.; Brown, M. F.; Chen, J. M.; Hayward, M. M.; Noe, M. C.; Obach, R. S.; Philippe, L.; Shanmugasundaram, V.; Shapiro, M. J.; Starr, J.; Stroh, J.; Che, Y. Chemical and Computational Methods for the Characterization of Covalent Reactive Groups for the Prospective Design of Irreversible Inhibitors. *J. Med. Chem.* **2014**, *57* (23), 10072–10079. https://doi.org/10.1021/jm501412a.

(17) Lonsdale, R.; Burgess, J.; Colclough, N.; Davies, N. L.; Lenz, E. M.; Orton, A. L.; Ward, R. A. Expanding the Armory: Predicting and Tuning Covalent Warhead Reactivity. *J. Chem. Inf. Model.* **2017**, *57* (12), 3124–3137. https://doi.org/10.1021/acs.jcim.7b00553.

(18) Ghosh, A. K.; Brindisi, M. Organic Carbamates in Drug Design and Medicinal Chemistry. *J. Med. Chem.* **2015**, *58* (7), 2895–2940. https://doi.org/10.1021/jm501371s.

(19) Luo, Y. L. Mechanism-Based and Computational-Driven Covalent Drug Design. *J. Chem. Inf. Model.* **2021**, *61* (11), 5307–5311. https://doi.org/10.1021/acs.jcim.1c01278.

(20) Thorarensen, A.; Balbo, P.; Banker, M. E.; Czerwinski, R. M.; Kuhn, M.; Maurer, T. S.; Telliez, J.-B.; Vincent, F.; Wittwer, A. J. The Advantages of Describing Covalent Inhibitor in Vitro Potencies by IC50 at a Fixed Time Point. IC50 Determination of Covalent Inhibitors Provides Meaningful Data to Medicinal Chemistry for SAR Optimization. *Bioorg. Med. Chem.* **2021**, *29*, 115865. https://doi.org/10.1016/j.bmc.2020.115865.

(21) Copeland, R. A. Irreversible Enzyme Inactivators. In *Evaluation of Enzyme Inhibitors in Drug Discovery*; John Wiley & Sons, Ltd, 2013; pp 345–382. https://doi.org/10.1002/9781118540398.ch9.

(22) Hoffmann, M.; Stiller, C.; Endres, E.; Scheiner, M.; Gunesch, S.; Sotriffer, C.; Maurice, T.; Decker, M. Highly Selective Butyrylcholinesterase Inhibitors with Tunable Duration of Action by Chemical Modification of Transferable Carbamate Units Exhibit Pronounced Neuroprotective Effect in an Alzheimer's Disease Mouse Model. *J. Med. Chem.* **2019**, *62* (20), 9116–9140. https://doi.org/10.1021/acs.jmedchem.9b01012.

(23) Groner, E.; Ashani, Y.; Schorer-Apelbaum, D.; Sterling, J.; Herzig, Y.; Weinstock, M. The Kinetics of Inhibition of Human Acetylcholinesterase and Butyrylcholinesterase by Two Series of Novel Carbamates. *Mol. Pharmacol.* **2007**, *71* (6), 1610–1617. https://doi.org/10.1124/mol.107.033928.

(24) Stojan, J. Rapid Mechanistic Evaluation and Parameter Estimation of Putative Inhibitors in a Single-Step Progress-Curve Analysis: The Case of Horse Butyrylcholinesterase. *Molecules* **2017**, *22* (8), 1248. https://doi.org/10.3390/molecules22081248.

(25) Bevc, S.; Konc, J.; Stojan, J.; Hodošček, M.; Penca, M.; Praprotnik, M.; Janežič, D. ENZO: A Web Tool for Derivation and Evaluation of Kinetic Models of Enzyme Catalyzed Reactions. *PLOS ONE* **2011**, *6* (7), e22265. https://doi.org/10.1371/journal.pone.0022265.

(26) Yu, Q.; Holloway, H. W.; Utsuki, T.; Brossi, A.; Greig, N. H. Synthesis of Novel Phenserine-Based-Selective Inhibitors of Butyrylcholinesterase for Alzheimer's Disease. *J. Med. Chem.* **1999**, *42* (10), 1855–1861. https://doi.org/10.1021/jm980459s.

(27) Perola, E.; Cellai, L.; Lamba, D.; Filocamo, L.; Brufani, M. Long Chain Analogs of Physostigmine as Potential Drugs for Alzheimer's Disease: New Insights into the Mechanism of Action in the Inhibition of Acetylcholinesterase. *Biochim. Biophys. Acta BBA - Protein Struct. Mol. Enzymol.* **1997**, *1343* (1), 41–50. https://doi.org/10.1016/S0167-4838(97)00133-7.

(28) Sawatzky, E.; Wehle, S.; Kling, B.; Wendrich, J.; Bringmann, G.; Sotriffer, C. A.; Heilmann, J.; Decker, M. Discovery of Highly Selective and Nanomolar Carbamate-Based Butyrylcholinesterase Inhibitors by Rational Investigation into Their Inhibition Mode. *J. Med. Chem.* **2016**, *59* (5), 2067–2082. https://doi.org/10.1021/acs.jmedchem.5b01674.

(29) Scheiner, M.; Sink, A.; Hoffmann, M.; Vrigneau, C.; Endres, E.; Carles, A.; Sotriffer, C.; Maurice, T.; Decker, M. Photoswitchable Pseudoirreversible Butyrylcholinesterase Inhibitors Allow Optical Control of Inhibition in Vitro and Enable Restoration of Cognition in an Alzheimer's Disease Mouse Model upon Irradiation. *J. Am. Chem. Soc.* **2022**, *144* (7), 3279–3284. https://doi.org/10.1021/jacs.1c13492.

(30) Venkatasubban, K. S.; Johnson, J. L.; Thomas, J. L.; Fauq, A.; Cusack, B.; Rosenberry, T. L. Decarbamoylation of Acetylcholinesterases Is Markedly Slowed as Carbamoyl Groups Increase in Size. *Arch. Biochem. Biophys.* **2018**, *655*, 67–74. https://doi.org/10.1016/j.abb.2018.08.006.

(31) Ballard, C. G.; Greig, N. H.; Guillozet-Bongaarts, A. L.; Enz, A.; Darvesh, S. Cholinesterases: Roles in the Brain During Health and Disease. *Curr. Alzheimer Res. 2* (3), 307–318.

(32) Gabriel, A. J.; Almeida, M. R.; Ribeiro, M. H.; Durães, J.; Tábuas-Pereira, M.; Pinheiro, A. C.; Pascoal, R.; Santana, I.; Baldeiras, I. Association between Butyrylcholinesterase and Cerebrospinal Fluid Biomarkers in Alzheimer's Disease Patients. *Neurosci. Lett.* **2017**, *641*, 101–106. https://doi.org/10.1016/j.neulet.2017.01.036.

(33) Moore, S. W.; Johnson, G. Acetylcholinesterase in Hirschsprung's Disease. *Pediatr. Surg. Int.* **2005**, *21* (4), 255–263. https://doi.org/10.1007/s00383-005-1383-z.

(34) Agrawal, R. K.; Kakkar, N.; Vasishta, R. K.; Kumari, V.; Samujh, R.; Rao, K. L. N. Acetylcholinesterase Histochemistry (AChE) - A Helpful Technique in the Diagnosis and in Aiding the Operative Procedures of Hirschsprung Disease. *Diagn. Pathol.* **2015**, *10* (1), 208. https://doi.org/10.1186/s13000-015-0443-5.

(35) Thorne, M. W. D.; Cash, M. K.; Reid, G. A.; Burley, D. E.; Luke, D.; Pottie, I. R.; Darvesh, S. Imaging Butyrylcholinesterase in Multiple Sclerosis. *Mol. Imaging Biol.* **2021**, *23* (1), 127–138. https://doi.org/10.1007/s11307-020-01540-6.

(36) Darvesh, S.; LeBlanc, A. M.; Macdonald, I. R.; Reid, G. A.; Bhan, V.; Macaulay, R. J.; Fisk, J. D. Butyrylcholinesterase Activity in Multiple Sclerosis Neuropathology. *Chem. Biol. Interact.* **2010**, *187* (1), 425–431. https://doi.org/10.1016/j.cbi.2010.01.037.

(37) Chao, S.; Krejci, E.; Bernard, V.; Leroy, J.; Jean, L.; Renard, P.-Y. A Selective and Sensitive Near-Infrared Fluorescent Probe for Acetylcholinesterase Imaging. *Chem. Commun.* **2016**, *52* (77), 11599–11602. https://doi.org/10.1039/C6CC05936H.

(38) Ma, Y.; Gao, W.; Ma, S.; Liu, Y.; Lin, W. Observation of the Elevation of Cholinesterase Activity in Brain Glioma by a Near-Infrared Emission Chemsensor. *Anal. Chem.* **2020**, *92* (19), 13405–13410. https://doi.org/10.1021/acs.analchem.0c02770.

(39) Wu, X.; An, J. M.; Shang, J.; Huh, E.; Qi, S.; Lee, E.; Li, H.; Kim, G.; Ma, H.; Oh, M. S.; Kim, D.; Yoon, J. A Molecular Approach to Rationally Constructing Specific Fluorogenic Substrates for the Detection of Acetylcholinesterase Activity in Live Cells, Mice Brains and Tissues. *Chem. Sci.* **2020**, *11* (41), 11285–11292. https://doi.org/10.1039/D0SC04213G.

(40) Xiang, C.; Dirak, M.; Luo, Y.; Peng, Y.; Cai, L.; Gong, P.; Zhang, P.; Kolemen, S. A Responsive AIE-Active Fluorescent Probe for Visualization of Acetylcholinesterase Activity in Vitro and in Vivo. *Mater. Chem. Front.* **2022**, *6* (11), 1515–1521. https://doi.org/10.1039/D2QM00239F.

(41) Fortibui, M. M.; Jang, M.; Lee, S.; Ryoo, I.-J.; Ahn, J. S.; Ko, S.-K.; Kim, J. Near-Infrared Fluorescence Probe for Specific Detection of Acetylcholinesterase and Imaging in Live

Cells and Zebrafish. *ACS Appl. Bio Mater.* **2022**, *5* (5), 2232–2239. https://doi.org/10.1021/acsabm.2c00084.

(42) Wang, X.; Li, P.; Ding, Q.; Wu, C.; Zhang, W.; Tang, B. Observation of Acetylcholinesterase in Stress-Induced Depression Phenotypes by Two-Photon Fluorescence Imaging in the Mouse Brain. *J. Am. Chem. Soc.* **2019**, *141* (5), 2061–2068. https://doi.org/10.1021/jacs.8b11414.

(43) Yang, Y.; Zhang, L.; Wang, J.; Cao, Y.; Qin, W.; Liu, Y. Real-Time Fluorescent Determination and Biological Imaging in Living Models via a Butyrylcholinesterase-Activated Fluorescent Probe. *Dyes Pigments* **2022**, 110596. https://doi.org/10.1016/j.dyepig.2022.110596.

(44) Xiang, C.; Xiang, J.; Yang, X.; Li, C.; Zhou, L.; Jiang, D.; Peng, Y.; Xu, Z.; Deng, G.; Zhu, B.; Zhang, P.; Cai, L.; Gong, P. Ratiometric Imaging of Butyrylcholinesterase Activity in Mice with Nonalcoholic Fatty Liver Using an AIE-Based Fluorescent Probe. *J. Mater. Chem. B* **2022**, *10* (22), 4254–4260. https://doi.org/10.1039/D2TB00422D.

(45) Zhang, Q.; Fu, C.; Guo, X.; Gao, J.; Zhang, P.; Ding, C. Fluorescent Determination of Butyrylcholinesterase Activity and Its Application in Biological Imaging and Pesticide Residue Detection. *ACS Sens.* **2021**, *6* (3), 1138–1146. https://doi.org/10.1021/acssensors.0c02398.

(46) Wang, L.; Du, C.; Liu, H.; Qiu, W.; Lu, X.; Hu, Y.; Li, Y.; Sun, T.; Chen, Y.; Sun, H. A Practical and High-Affinity Fluorescent Probe for Butyrylcholinesterase: A Good Strategy for Binding Affinity Characterization. *Chin. J. Chem.* **2022**, *40* (11), 1285–1292. https://doi.org/10.1002/cjoc.202100910.

(47) Liu, S.-Y.; Xiong, H.; Yang, J.-Q.; Yang, S.-H.; Li, Y.; Yang, W.-C.; Yang, G.-F. Discovery of Butyrylcholinesterase-Activated Near-Infrared Fluorogenic Probe for Live-Cell and In Vivo Imaging. *ACS Sens.* **2018**, *3* (10), 2118–2128. https://doi.org/10.1021/acssensors.8b00697.

(48) Koelle, G. B.; Friedenwald, J. S. A Histochemical Method for Localizing Cholinesterase Activity. *Proc. Soc. Exp. Biol. Med.* **1949**, *70* (4), 617–622. https://doi.org/10.3181/00379727-70-17013.

(49) Renard, P.-Y.; Jean, L. Probing the Cholinergic System to Understand Neurodegenerative Diseases. *Future Med. Chem.* **2017**, *9* (2), 131–133. https://doi.org/10.4155/fmc-2016-0213.

(50) Yu, Q.; Liao, J.; Xu, F.; Yuan, X.; Xiong, X.; Xiao, T.; Yu, H.; Huang, K. Developments of Spectroscopic Biosensors for Cholinesterase and Its Inhibitors in the Last Decade: An Overview. *Appl. Spectrosc. Rev.* **2021**, *0* (0), 1–25. https://doi.org/10.1080/05704928.2021.1990080.

(51) Rajapaksha, A. A.; Fu, Y.-X.; Guo, W. Y.; Liu, S.-Y.; Li, Z.-W.; Xiong, C.-Q.; Yang, W.-C.; Yang, G.-F. Review on the Recent Progress in the Development of Fluorescent Probes Targeting Enzymes. *Methods Appl. Fluoresc.* **2021**, *9* (3), 032001. https://doi.org/10.1088/2050-6120/abf988.

(52) Meden, A.; Knez, D.; Brazzolotto, X.; Nachon, F.; Dias, J.; Svete, J.; Stojan, J.; Grošelj, U.; Gobec, S. From Tryptophan-Based Amides to Tertiary Amines: Optimization of a Butyrylcholinesterase Inhibitor Series. *Eur. J. Med. Chem.* **2022**, *234*, 114248. https://doi.org/10.1016/j.ejmech.2022.114248.

(53) Speers, A. E.; Cravatt, B. F. Profiling Enzyme Activities In Vivo Using Click Chemistry Methods. *Chem. Biol.* **2004**, *11* (4), 535–546. https://doi.org/10.1016/j.chembiol.2004.03.012.

(54) Parker, C. G.; Pratt, M. R. Click Chemistry in Proteomic Investigations. *Cell* **2020**, *180* (4), 605–632. https://doi.org/10.1016/j.cell.2020.01.025.

(55) Bourne, Y.; Kolb, H. C.; Radić, Z.; Sharpless, K. B.; Taylor, P.; Marchot, P. Freeze-Frame Inhibitor Captures Acetylcholinesterase in a Unique Conformation. *Proc. Natl. Acad. Sci.* **2004**, *101* (6), 1449–1454. https://doi.org/10.1073/pnas.0308206100.

(56) Lewis, W. G.; Green, L. G.; Grynszpan, F.; Radić, Z.; Carlier, P. R.; Taylor, P.; Finn, M. G.; Sharpless, K. B. Click Chemistry In Situ: Acetylcholinesterase as a Reaction Vessel for the Selective Assembly of a Femtomolar Inhibitor from an Array of Building Blocks. *Angew. Chem. Int. Ed.* **2002**, *41* (6), 1053–1057. https://doi.org/10.1002/1521-3773(20020315)41:6<1053::AID-ANIE1053>3.0.CO;2-4.

(57) Manetsch, R.; Krasiński, A.; Radić, Z.; Raushel, J.; Taylor, P.; Sharpless, K. B.; Kolb, H. C. In Situ Click Chemistry: Enzyme Inhibitors Made to Their Own Specifications. *J. Am. Chem. Soc.* **2004**, *126* (40), 12809–12818. https://doi.org/10.1021/ja046382g.

(58) Grzyb, J. A.; Shen, M.; Yoshina-Ishii, C.; Chi, W.; Brown, R. S.; Batey, R. A. Carbamoylimidazolium and Thiocarbamoylimidazolium Salts: Novel Reagents for the Synthesis of Ureas, Thioureas, Carbamates, Thiocarbamates and Amides. *Tetrahedron* **2005**, *61* (30), 7153–7175. https://doi.org/10.1016/j.tet.2005.05.056.

(59) Singh, J.; Petter, R. C.; Baillie, T. A.; Whitty, A. The Resurgence of Covalent Drugs. *Nat. Rev. Drug Discov.* **2011**, *10* (4), 307–317. https://doi.org/10.1038/nrd3410.

(60) Brazzolotto, X.; Igert, A.; Guillon, V.; Santoni, G.; Nachon, F. Bacterial Expression of Human Butyrylcholinesterase as a Tool for Nerve Agent Bioscavengers Development. *Molecules* **2017**, *22* (11), 1828. https://doi.org/10.3390/molecules22111828.

(61) *ExPASy - ProtParam tool*. https://web.expasy.org/protparam/ (accessed 2022-07-25).

(62) Arsov, Z.; Švajger, U.; Mravljak, J.; Pajk, S.; Kotar, A.; Urbančič, I.; Štrancar, J.; Anderluh, M. Internalization and Accumulation in Dendritic Cells of a Small PH-Activatable Glycomimetic Fluorescent Probe as Revealed by Spectral Detection. *ChemBioChem* **2015**, *16* (18), 2660–2667. https://doi.org/10.1002/cbic.201500376.

(63) Komloova, M.; Horova, A.; Hrabinova, M.; Jun, D.; Dolezal, M.; Vinsova, J.; Kuca, K.; Musilek, K. Preparation, in Vitro Evaluation and Molecular Modelling of Pyridinium–Quinolinium/Isoquinolinium Non-Symmetrical Bisquaternary Cholinesterase Inhibitors. *Bioorg. Med. Chem. Lett.* **2013**, *23* (24), 6663–6666. https://doi.org/10.1016/j.bmcl.2013.10.043.

(64) Kolarich, D.; Weber, A.; Pabst, M.; Stadlmann, J.; Teschner, W.; Ehrlich, H.; Schwarz, H.-P.; Altmann, F. Glycoproteomic Characterization of Butyrylcholinesterase from Human Plasma. *PROTEOMICS* **2008**, *8* (2), 254–263. https://doi.org/10.1002/pmic.200700720.

(65) Li, B.; Sedlacek, M.; Manoharan, I.; Boopathy, R.; Duysen, E. G.; Masson, P.; Lockridge, O. Butyrylcholinesterase, Paraoxonase, and Albumin Esterase, but Not Carboxylesterase, Are Present in Human Plasma. *Biochem. Pharmacol.* **2005**, *70* (11), 1673–1684. https://doi.org/10.1016/j.bcp.2005.09.002.

(66) Košak, U.; Brus, B.; Knez, D.; Šink, R.; Žakelj, S.; Trontelj, J.; Pišlar, A.; Šlenc, J.; Gobec, M.; Živin, M.; Tratnjek, L.; Perše, M.; Sałat, K.; Podkowa, A.; Filipek, B.; Nachon, F.; Brazzolotto, X.; Więckowska, A.; Malawska, B.; Stojan, J.; Raščan, I. M.; Kos, J.; Coquelle, N.; Colletier, J.-P.; Gobec, S. Development of an In-Vivo Active Reversible Butyrylcholinesterase Inhibitor. *Sci. Rep.* **2016**, *6*, 39495.

(67) Speers, A. E.; Cravatt, B. F. Activity-Based Protein Profiling (ABPP) and Click Chemistry (CC)–ABPP by MudPIT Mass Spectrometry. *Curr. Protoc. Chem. Biol.* **2009**, *1* (1), 29–41. https://doi.org/10.1002/9780470559277.ch090138.

(68) Pajk, S.; Knez, D.; Košak, U.; Zorović, M.; Brazzolotto, X.; Coquelle, N.; Nachon, F.; Colletier, J.-P.; Živin, M.; Stojan, J.; Gobec, S. Development of Potent Reversible Selective Inhibitors of Butyrylcholinesterase as Fluorescent Probes. *J. Enzyme Inhib. Med. Chem.* **2020**, *35* (1), 498–505. https://doi.org/10.1080/14756366.2019.1710502.

(69) Nachon, F.; Nicolet, Y.; Viguié, N.; Masson, P.; Fontecilla-Camps, J. C.; Lockridge, O. Engineering of a Monomeric and Low-Glycosylated Form of Human Butyrylcholinesterase. *Eur. J. Biochem.* **2002**, *269* (2), 630–637. https://doi.org/10.1046/j.0014-2956.2001.02692.x.

(70) Brazzolotto, X.; Wandhammer, M.; Ronco, C.; Trovaslet, M.; Jean, L.; Lockridge, O.; Renard, P.-Y.; Nachon, F. Human Butyrylcholinesterase Produced in Insect Cells: Huprine-Based Affinity Purification and Crystal Structure. *FEBS J.* **2012**, *279* (16), 2905–2916. https://doi.org/10.1111/j.1742-4658.2012.08672.x.

(71) Kabsch, W. XDS. *Acta Crystallogr. D Biol. Crystallogr.* **2010**, *66* (2), 125–132. https://doi.org/10.1107/S0907444909047337.

(72) Afonine, P. V.; Poon, B. K.; Read, R. J.; Sobolev, O. V.; Terwilliger, T. C.; Urzhumtsev, A.; Adams, P. D. Real-Space Refinement in PHENIX for Cryo-EM and Crystallography. *Acta Crystallogr. Sect. Struct. Biol.* **2018**, *74* (6), 531–544. https://doi.org/10.1107/S2059798318006551.

(73) Moriarty, N. W.; Grosse-Kunstleve, R. W.; Adams, P. D. Electronic Ligand Builder and Optimization Workbench (ELBOW): A Tool for Ligand Coordinate and Restraint Generation. *Acta Crystallogr. Sect. D* **2009**, *65* (10), 1074–1080. https://doi.org/10.1107/S0907444909029436.

(74) Emsley, P.; Lohkamp, B.; Scott, W. G.; Cowtan, K. Features and Development of It Coot. *Acta Crystallogr. Sect. D* **2010**, *66* (4), 486–501. https://doi.org/10.1107/S0907444910007493.

(75) Wenig, P.; Odermatt, J. OpenChrom: A Cross-Platform Open Source Software for the Mass Spectrometric Analysis of Chromatographic Data. *BMC Bioinformatics* **2010**, *11* (1), 405. https://doi.org/10.1186/1471-2105-11-405.

(76) Marty, M. T.; Baldwin, A. J.; Marklund, E. G.; Hochberg, G. K. A.; Benesch, J. L. P.; Robinson, C. V. Bayesian Deconvolution of Mass and Ion Mobility Spectra: From Binary Interactions to Polydisperse Ensembles. *Anal. Chem.* **2015**, *87* (8), 4370–4376. https://doi.org/10.1021/acs.analchem.5b00140.

(77) Bowers, K. J.; Chow, E.; Xu, H.; Dror, R. O.; Eastwood, M. P.; Gregersen, B. A.; Klepeis, J. L.; Kolossvary, I.; Moraes, M. A.; Sacerdoti, F. D.; Salmon, J. K.; Shan, Y.; Shaw, D. E. Scalable Algorithms for Molecular Dynamics Simulations on Commodity Clusters. In *Proceedings of the 2006 ACM/IEEE conference on Supercomputing*; SC '06; Association for Computing Machinery: New York, NY, USA, 2006; pp 84-es. https://doi.org/10.1145/1188455.1188544.

(78) Shelley, J. C.; Cholleti, A.; Frye, L. L.; Greenwood, J. R.; Timlin, M. R.; Uchimaya, M. Epik: A Software Program for PKaprediction and Protonation State Generation for Drug-like Molecules. *J. Comput. Aided Mol. Des.* **2007**, *21* (12), 681–691. https://doi.org/10.1007/s10822-007-9133-z.

(79) Olsson, M. H. M.; Søndergaard, C. R.; Rostkowski, M.; Jensen, J. H. PROPKA3: Consistent Treatment of Internal and Surface Residues in Empirical PKa Predictions. *J. Chem. Theory Comput.* **2011**, *7* (2), 525–537. https://doi.org/10.1021/ct100578z.

(80) Jorgensen, W. L.; Maxwell, D. S.; Tirado-Rives, J. Development and Testing of the OPLS All-Atom Force Field on Conformational Energetics and Properties of Organic Liquids. *J. Am. Chem. Soc.* **1996**, *118* (45), 11225–11236. https://doi.org/10.1021/ja9621760.

(81) Banks, J. L.; Beard, H. S.; Cao, Y.; Cho, A. E.; Damm, W.; Farid, R.; Felts, A. K.; Halgren, T. A.; Mainz, D. T.; Maple, J. R.; Murphy, R.; Philipp, D. M.; Repasky, M. P.; Zhang, L. Y.; Berne, B. J.; Friesner, R. A.; Gallicchio, E.; Levy, R. M. Integrated Modeling Program, Applied Chemical Theory (IMPACT). *J. Comput. Chem.* **2005**, *26* (16), 1752–1780. https://doi.org/10.1002/jcc.20292.

(82) Friesner, R. A.; Murphy, R. B.; Repasky, M. P.; Frye, L. L.; Greenwood, J. R.; Halgren, T. A.; Sanschagrin, P. C.; Mainz, D. T. Extra Precision Glide: Docking and Scoring Incorporating a Model of Hydrophobic Enclosure for Protein-Ligand Complexes. *J. Med. Chem.* **2006**, *49* (21), 6177–6196. https://doi.org/10.1021/jm051256o.

(83) Zhu, K.; Borrelli, K. W.; Greenwood, J. R.; Day, T.; Abel, R.; Farid, R. S.; Harder, E. Docking Covalent Inhibitors: A Parameter Free Approach to Pose Prediction and Scoring. *J. Chem. Inf. Model.* **2014**, *54* (7), 1932–1940. https://doi.org/10.1021/ci500118s.

(84) Jorgensen, W. L.; Chandrasekhar, J.; Madura, J. D.; Impey, R. W.; Klein, M. L. Comparison of Simple Potential Functions for Simulating Liquid Water. *J. Chem. Phys.* **1983**, *79* (2), 926–935. https://doi.org/10.1063/1.445869.

(85) Bochevarov, A. D.; Harder, E.; Hughes, T. F.; Greenwood, J. R.; Braden, D. A.; Philipp, D. M.; Rinaldo, D.; Halls, M. D.; Zhang, J.; Friesner, R. A. Jaguar: A High-Performance Quantum Chemistry Software Program with Strengths in Life and Materials Sciences. *Int. J. Quantum Chem.* **2013**, *113* (18), 2110–2142. https://doi.org/10.1002/qua.24481.

(86) Meden, A.; Knez, D.; Jukič, M.; Brazzolotto, X.; Gršič, M.; Pišlar, A.; Zahirović, A.; Kos, J.; Nachon, F.; Svete, J.; Gobec, S.; Grošelj, U. Tryptophan-Derived Butyrylcholinesterase Inhibitors as Promising Leads against Alzheimer's Disease. *Chem. Commun.* **2019**, *55* (26), 3765–3768. https://doi.org/10.1039/C9CC01330J.

(87) Harada, H.; Fujii, A.; Kato, S. An Efficient and Practical Synthesis of N , N -Diethyl-7-Indolyloxyacetamide via 7-Hydroxyindole. *Synth. Commun.* **2003**, *33* (3), 507–514. https://doi.org/10.1081/SCC-120015783.

(88) Pearson, S. E.; Fillery, S. M.; Goldberg, K.; Demeritt, J. E.; Eden, J.; Finlayson, J.; Patel, A. Synthesis of Indole-Dihydroisoquinoline Sulfonyl Ureas via Three-Component Reactions. *Synthesis* **2018**, *50* (24), 4963–4981. https://doi.org/10.1055/s-0037-1610223.

(89) Nudelman, A.; Weinstock-Rosin, M. Indole, Indoline Derivatives, Compositions Comprising Them and Uses Thereof. WO2013150529A2, October 10, 2013.

(90) Khanna, A.; Maung, C.; Johnson, K. R.; Luong, T. T.; Van Vranken, D. L. Carbenylative Amination with N-Tosylhydrazones. *Org. Lett.* **2012**, *14* (12), 3233–3235. https://doi.org/10.1021/ol301385g.

(91) Narasimhan, S.; Mohan, H.; Palani, N. An Improved Procedure for the Synthesis of Terminal and Internal Alkynes from 10-Undecenoic Acid. *Synth. Commun.* **1991**, *21* (18–19), 1941–1949. https://doi.org/10.1080/00397919108021786.

(92) Epsztein, R.; Le Goff, N. Synthese de bases de mannich acetyleniques cycliques. *Tetrahedron Lett.* **1985**, *26* (27), 3203–3206. https://doi.org/10.1016/S0040-4039(00)98152-8.

(93) Chukhajian, E. O.; Ayrapetyan, L. V.; Mkrtchyan, H. S.; Panosyan, H. A. Synthesis of Mixed Secondary and Tertiary Amines. *Russ. J. Org. Chem.* **2020**, *56* (2), 353–355. https://doi.org/10.1134/S1070428020010311.

(94) Veguillas, M.; Rosair, G. M.; Bebbington, M. W. P.; Lee, A.-L. Silver Effect in Regiodivergent Gold-Catalyzed Hydroaminations. *ACS Catal.* **2019**, *9* (3), 2552–2557. https://doi.org/10.1021/acscatal.9b00249.

(95) García-Rubio, S.; Wilson, C. D.; Renner, D. A.; Rosser, J. O.; Patra, D.; Reid, J. G.; Pines, S. H. An Improved Process for the Preparation of Trimethylhydrazine and Its Coupling with an Activated Acid Intermediate. *Org. Process Res. Dev.* **2004**, *8* (3), 360–362. https://doi.org/10.1021/op0342022.

(96) Tahtaoui, C.; Parrot, I.; Klotz, P.; Guillier, F.; Galzi, J.-L.; Hibert, M.; Ilien, B. Fluorescent Pirenzepine Derivatives as Potential Bitopic Ligands of the Human M1 Muscarinic Receptor. *J. Med. Chem.* **2004**, *47* (17), 4300–4315. https://doi.org/10.1021/jm040800a.
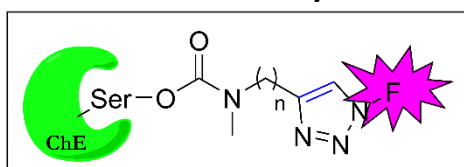
For Table of Contents Only:
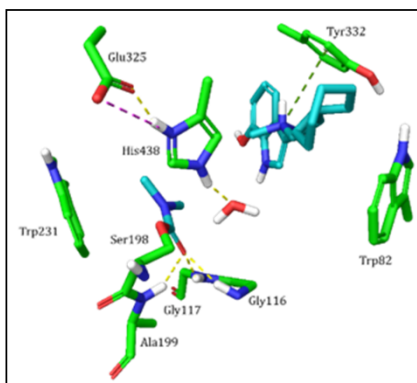
TIFF 1200 dpi:

pseudo-irreversible ChEI:
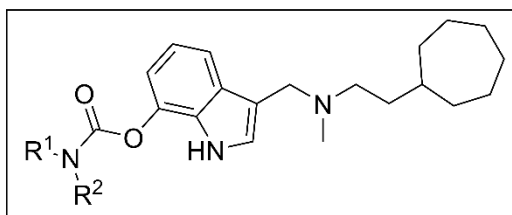
SAR study

fluorescent labelling of ChEs

proof of covalent binding